https://doi.org/10.1016/j.rser.2021.111313

Research progress on utilization of phase change materials in photovoltaic/thermal systems: A critical review

Qinghua Yu[a, b, *], Xi Chen[c], Hongxing Yang[a, #]

[a] Renewable Energy Research Group, Department of Building Services Engineering, The Hong Kong Polytechnic University, Hong Kong

[b] School of Automotive Engineering, Wuhan University of Technology, Wuhan, PR China

[c] School of Science and Technology, The Open University of Hong Kong, Hong Kong

[*]Corresponding author. E-mail address: qinghua.yu@polyu.edu.hk (Q. Yu)

[#]Corresponding author. E-mail address: hong-xing.yang@polyu.edu.hk (H. Yang)

Abstract

A photovoltaic/thermal (PV/T) technology, producing electricity and heat simultaneously, has attracted extensive attention. Integration of phase change materials (PCMs) into PV/T systems as auxiliary cooling media or/and heat storage media to improve the system performances has been prevalent in recent years. This paper aims to critically and comprehensively review the research progress concerning utilization of PCMs in PV/T systems. The adopted performance evaluation indexes and applied PCMs in various PV/T systems are gathered and analysed. The configurations and effects of bulk PCMs in standalone PV/T modules, building-integrated PV/T systems and PV/T systems integrated with other energy conversion technologies are elaborated with special attention paid to the microencapsulated PCM (MPCM) slurry applied in PV/T modules. The effects of thermophysical properties and mass of PCM/MPCM, operation parameters of working fluids, and environmental conditions are also discussed, whilst heat transfer enhancement approaches for PV/T-PCM modules are explored. It has been identified that the integration of PCMs can effectively elevate the system performances when the phase change temperature and operation parameters are carefully tailored according to environmental conditions. Finally, research prospects and opportunities are proposed in terms of material fabrication and modification, system integration, model development as well as performance analysis. The review can provide crucial references for high-efficiency PV/T-PCM system design and further development of relevant technologies.

Highlights

• PCMs adopted in PV/T systems as well as the system performances are summarized.

• Configurations and roles of bulk or microencapsulated PCMs in PV/T are elaborated.

• Effects of key parameters on PV/T performance with PCMs are comprehensively analyzed.

• Use of PCMs in building-integrated PV/T helps to flexibly adjust spatial energy flow.

• PV/T with PCMs can be flexibly integrated with other energy conversion methods.

Keywords: Phase change material; Photovoltaic/thermal; Solar energy; Building-integrated.

Word count: 9975 (excluding title, author names and affiliations, abstract, highlights, keywords, contents, table/figure and their captions, acknowledgments and references).

Contents

1. Introduction 5
2. Performance evaluation indexes of PV/T systems 8
3. Thermophysical properties of PCMs used in PV/T systems 10
4. Utilization of bulk PCMs in PV/T modules 14
4.1 Configurations of PV/T modules integrated with bulk PCMs 14
4.2 Roles of bulk PCMs integrated into PV/T modules 17
4.3 Effects of key parameters on PV/T modules with bulk PCMs 20
4.4 Heat transfer enhancement methods for PV/T modules with bulk PCMs 25
4.5 Economic analysis for PV/T modules with bulk PCMs 30
5. Utilization of MPCM slurry in PV/T modules 31
5.1 Performance comparison between PV/T with MPCM slurry and water 32
5.2 Effects of key parameters on PV/T modules with MPCM slurry 34
6. Development of BIPV/T-PCM systems 36
6.1 BIPV/T on the roof 37
6.2 BIPV/T on the façade 40
7. PV/T-PCM integrated with other energy conversion technologies 44
7.1 Heat pipe 44
7.2 Thermoelectric device 46
7.3 Heat pump 47
7.4 Ejector refrigeration cycle 48
7.5 Solar still for fresh water production 49
7.6 Proton Exchange Membrane electrolyzer for hydrogen production 50
8. Conclusions and Outlook 51
8.1 Summary of conclusions 51
8.2 Outlook for PV/T-PCM technologies 57
Acknowledgements 58
References 59

1. Introduction

A photovoltaic/thermal (PV/T) technology, combining solar PV and photothermal conversions, has proven to be a promising solution to better exploit solar energy [1-3]. PV/T modules can generate electricity and heat simultaneously, whilst they enable low operating temperatures of the PV panels for maintaining high photoelectric conversion efficiencies. Therefore, they can provide higher power and energy output on the same area of solar radiation compared to conventional solar thermal collectors or PV panels [4, 5].

PV/T modules can be classified from various viewpoints as summarized in Table 1. For example, in light of the solar radiation collection mode, they could be flat-plate, concentrated, biracial or spectrum splitting type; on the basis of the installation mode, they can be divided into standalone and building-integrated type; according to the working fluid, they may be air-based, water-based or nanofluid-based type.

Table 1 The classification of PV/T modules.

Perspective	Classification of PV/T modules
Radiation collection mode	1. Flat-plate PV/T (FPPV/T) [6]
	2. Concentrated PV/T (CPV/T) [7]
	3. Bifacial PV/T (BPV/T) [8]
	4. Spectrum splitting PV/T (SSPV/T) [9, 10]
Installation mode [7]	1. Standalone PV/T (SPV/T)
	2. Building-integrated PV/T (BIPV/T)
Working fluid [7]	1. Air-based PV/T (APV/T)
	2. Water-based PV/T (WPV/T)
	3. Nanofluid-based PV/T (NPV/T)
Use of special heat transfer device [7]	1. Heat pipe-based PV/T
	2. Microchannel-based PV/T
	3. Jet impingement-based PV/T
Solar cell material [7, 11]	1. Crystalline silicon (c-Si)-based PV/T
	2. Amorphous silicon (a-Si)-based PV/T
	3. Cadmium telluride (CdTe)-based PV/T
	4. Copper indium gallium selenide (CIGS)-based PV/T
	5. Group III-V material-based PV/T (Such as GaAs)

Fig. 1 demonstrates typical configurations of air-based and water-based PV/T modules. Both of them are flat-plate types and consist of a glass cover, a PV panel, an absorber plate and a thermal insulation layer. The glass cover is generally made of a transparent toughened glass placed above the PV panel while the thermal insulation layer is used to mainly cover the rear surface of the absorber plate. In the air-based PV/T module, an air flow channel is formed between the absorber plate and the PV panel to cool the PV panel and absorb heat. In the water-based PV/T module, the absorber plate is attached beneath the PV panel to collect heat while several ducts serving as the water channels are evenly welded on the back surface of the absorber plate for heat absorption and transportation. Configurations of most PV/T modules using other liquid working fluids are similar to that of the water-based PV/T module. Although a spectrum splitting PV/T module also adopts a liquid working fluid (e.g. water [12] or nanofluid [13]), it has a significantly different configuration, where the working fluid inside a transparent channel is placed above the PV panel to serve as a spectral filter [14]; The spectral filter absorbs the ineffective spectrum for PV cells to prevent the PV panel overheating and provide heat [15]. Other types of PV/T modules as listed in Table 1 will be described in detail with the utilization of phase change materials (PCMs) in the following sections.

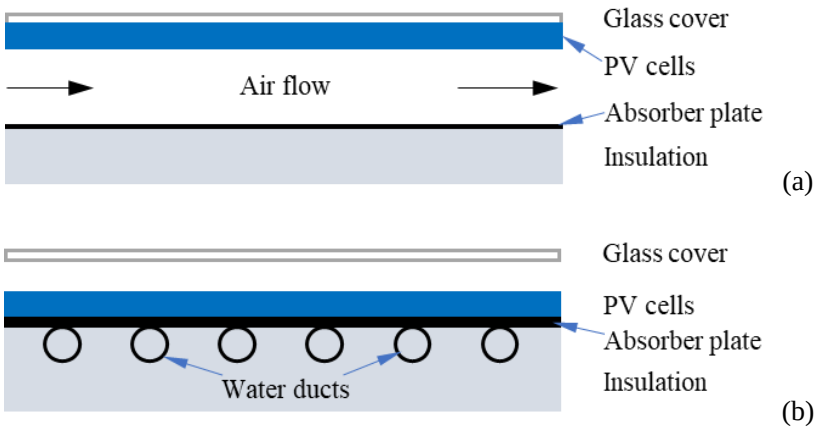

Fig. 1 Schematic diagrams of a typical configuration of (a) air-based PV/T and (b) water-based PV/T

In recent years, PCMs have been widely utilized in PV/T systems to further reduce the PV panel temperature and its distribution nonuniformity, augment the overall energy

conversion efficiency and elevate the operation flexibility as well as diminish the installation space requirement. The above potential improvements can be achieved based on the advantages of PCMs, which have high latent heat absorption capacity with quite a small temperature variation during the solid-liquid phase transition process [16]. Thus, PCMs show a high energy storage density as illustrated in Fig. 2. PCMs have a wide range of types [17], utilization forms (bulk or microencapsulated) and integration methods in PV/T systems, while PV/T modules possess plenty of different structures or classifications and work under varying climate conditions, which make the efficient utilization of PCMs in PV/T systems very complicated. A critical review concerning the recent development of utilization of PCMs in PV/T systems is required, to clarify new and optimum designs of PV/T-PCM systems, suitable PCMs for various PV/T systems, optimal operation schemes as well as related techniques of enhanced heat transfer and energy harvesting.

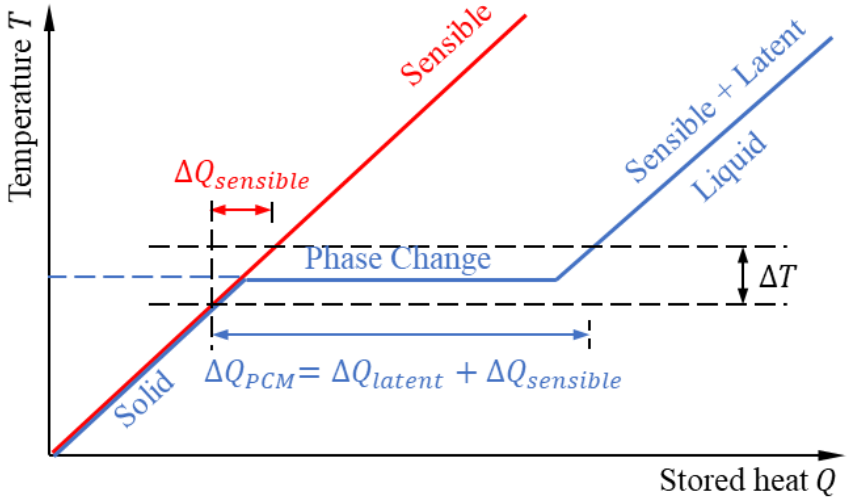

Fig. 2 The heat storage density ΔQ_{PCM} of PCM is much higher than the storage density $\Delta Q_{sensible}$ of sensible heat storage materials at small temperature intervals ΔT across phase change temperature. Most real PCMs show a small temperature region instead of a temperature during phase change.

Several reviews have been published on the study of PV/T [18-20]. Islam et al. [7] carried out an overview of preliminary research work of PCMs in PV/T systems with prospects of future research. Abdelrazik et al. [21] reviewed the design and cooling methods for PV/T

systems with special attention on the application of nanoparticles in the cooling fluids and PCM storage mediums. Jia et al. [22] analysed operation environments and applications suitable for various PV/T modules. Diwania et al. [23] reviewed the design modification and development of PV/T modules as well as their applications. Riaz et al. [24] discussed the integrations between PV/T modules and building facades. Although a few review papers partially involved the development of PCM-based PV/T technologies, no specialised review focusing on the utilization of PCMs in PV/T systems is available in the literature.

Therefore, this review attempts to comprehensively present the recent progress of PCM-based PV/T technologies to demonstrate their advantages and disadvantages with guiding further technology development. The organization of the rest of this paper is as follows: Section 2 outlines the performance evaluation indexes of PV/T systems. In Section 3, the thermophysical properties of the PCMs applied in various PV/T systems are summarized. Section 4 elaborates the utilization of bulk PCM in standalone PV/T modules including the configurations, roles of bulk PCMs, effects of key parameters on module performances and heat transfer enhancement methods as well as economic analysis. Section 5 elucidates the utilization of MPCM slurry in PV/T modules for performance improvements compared with the pure water-based cases. In Section 6, the impacts of PCMs integrated into various BIPV/T systems on building energy and indoor thermal environment are evaluated in detail. Section 7 provides the recent advances in the integration of PV/T-PCM with other energy conversion technologies. The paper ends with conclusions and a perspective for future research in PCM-based PV/T technologies in Section 8.

2. Performance evaluation indexes of PV/T systems

The performances of PV/T systems can be evaluated from multiple aspects, such as system noise, system weight, installation space, initial investment, maintenance cost and

energy performance. The performance evaluation indexes of PV/T systems are provided mainly from the aspect of energy performance in this paper, which are summarized in Table 2. The electrical power indicates the electricity-generating capability of the studied PV/T system under certain environmental conditions, while the thermal power indicates the corresponding heat-producing capability. The electrical efficiency and the thermal efficiency denote the photoelectric conversion ability and the photothermal conversion ability of the PV/T system, respectively. The overall energy efficiency stands for the overall energy conversion ability from solar radiation pear unit area. It is well known from thermodynamics that electrical energy has a higher grade than thermal energy. The former can be thoroughly converted into heat, while the latter can only be partially converted into electricity. Therefore, the primary-energy saving efficiency is introduced to indicate the overall energy performance of the system considering the energy grade difference between electrical and thermal energies [25]. Further, it is well known that the exergy (i.e. maximum useful work) can also be used to take the energy grade difference into account. The exergy efficiency is therefore proposed as another index to demonstrate the overall performance of PV/T systems. When MPCM slurry is applied as the working fluid, the pump power consumption for transporting the fluid is non-negligible and therefore a net efficiency is introduced to take the pump power consumption into account [26].

Table 2 Performance evaluation indexes of PV/T systems.

Performance Index	Equation
Electrical power	$P_e = V_c \times I_c$
Thermal power (useful heat)	$P_{th} = \int_{T_i}^{T_o} \dot{m} c_p dT$ or $= \int_{T_i}^{T_o} \dot{m} c_p dT + P_{pcm}$
Electrical efficiency	$\eta_e = \frac{P_e}{Q_s \times A_{PV}}$
Thermal efficiency	$\eta_{th} = \frac{P_{th}}{Q_s \times A_{AP}}$
Overall energy efficiency	$^{a}\eta_{en} = \eta_{th} + \eta_e$ or $^{b}\eta_{en} = \eta_{th} + R_a \eta_e$
Primary-energy saving efficiency	$^{a}\eta_{pe} = \eta_{th} + \eta_e / \eta_{plant}$
	or $^{b}\eta_{pe} = \eta_{th} + R_a \eta_e / \eta_{plant}$
Net efficiency	$\eta_{net} = \frac{P_e + P_{th} - P_p}{Q_s \times A_{PV}}$
Exergy efficiency	$^{a}\eta_{ex} = (\dot{E}x_e + \dot{E}x_{th}) / \dot{E}x_{solar}$
	or $^{b}\eta_{ex} = \eta_e + \eta_{th}(1 - T_a / T_o)$

Note: V_c– output voltage of PV cell; I_c– output current of PV cell; T_i– inlet fluid temperature; T_o– outlet fluid temperature; $\dot{m}$– mass flow rate; c_p– specific heat; P_{pcm}– the thermal power absorbed by PCM; Q_s– solar radiation intensity; A_{PV}– area of PV panel; A_{AP}– area of absorber plate; ^{a} or ^{b}– indicator for different calculation or definition expressions; R_a– ratio of the PV panel area to the absorber plate area; η_{plant}– average efficiency of conventional power plants (=38%); P_p– pump power consumption; $\dot{E}x_e$– electrical exergy; $\dot{E}x_{th}$– thermal exergy; $\dot{E}x_{solar}$– solar radiation exergy; T_a– ambient temperature.

3. Thermophysical properties of PCMs used in PV/T systems

Selecting suitable PCMs is very essential for their utilization in PV/T systems to improve system performances. The thermophysical properties of PCMs used in PV/T systems from the literature are summarized in Table 3. Various PCMs with different properties were used in PV/T systems, so that analyses on different aspects of PCMs are necessary to make them viable for achieving better energy performance of PV/T systems. Most studies available in the literature applied organic PCMs in PV/T systems including various types of paraffins, acids and their eutectic mixtures, while a small number of studies adopted inorganic hydrated salts or eutectic salts. Paraffins are the most easily available type of PCMs on the market with

excellent thermostability and fewer chemical issues. They all exhibit low thermal conductivities, which are around 0.2 W/m·K for organic PCMs and around 0.6 W/m·K for inorganic PCMs, respectively. Suitable heat transfer enhancement approaches are required within PCMs. Distributions of phase change temperature and latent heat for PCMs listed in Table 3 are illustrated in Fig. 3. Among all the adopted PCMs, the inorganic ones provide the highest phase change temperature or latent heat. Generally, the phase change temperatures of PCMs applied in FPPV/T systems are lower than those in CPV/T systems since higher operation temperatures are achieved in CPV/T systems. The former ones are within the range of 14–57 ºC, whilst the latter ones are within the range from 47 ºC to147 ºC. Under a super high operation temperature (e.g. 147 ºC) in CPV/T systems, a crystalline silicon-based cell was not suitable and other types of cells (e.g. GaAs cell) were required [27]. Furthermore, the latent heats of the adopted PCMs were distributed between 140 kJ/kg and 280 kJ/kg.

Table 3 Lists of PCMs used in PV/T systems in the literature.

PCM [Ref.]	Phase change temperature (°C)	Latent heat of fusion (kJ/kg)	Density (kg/m^3)	Specific heat capacity (kJ/kg·K)	Thermal conductivity (W/m·K)	Type of PV/T
Organic						
Paraffin C15 [28]	14	205	900 (s) / 760 (l)	2.52	N.A.	FPPV/T
Paraffin [29]	15	182	673	1.5	0.2	
Capric: palmitic acid [28, 30]	17.7–22.8	189–191	883	1.65	0.143	
Capric: palmitic acid [31]	22.5	173	870 (s) / 790 (l)	2.0 (s) / 2.3 (l)	0.14	
Paraffin RT20 [31]	25.7	140.3	880 (s) / 770 (l)	1.8 (s) / 2.4 (l)	0.2	
Paraffin RT25 [31, 32]	26.6	232	785 (s) / 749 (l)	1.4 (s) / 1.8 (l)	0.19 (s) / 0.18 (l)	
Paraffin [33]	28	210	860 (s) / 780 (l)	2.9 (s) / 2.1 (l)	0.24 (s) / 0.15 (l)	
Paraffin RT28 [34]	28	245	810	1.9	0.2	
Paraffin RT30 [35]	28	222	870 (s) / 760 (l)	2.4 (s) / 1.8 (l)	0.2	
Octadecane [36]	28	244	774	1.9	0.21	
Paraffin C18 [28]	29	244	900 (s) / 760 (l)	2.52	N.A.	
Capric acid [37, 38]	30.1	158–163	886	1.9 (s) / 2.1 (l)	0.149–0.153	
Paraffin RT31 [39]	27-31	169	880 (s) / 760 (l)	2	0.2	
Decanoic acid [40]	27-32	179.13	N.A.	N.A.	N.A.	
Paraffin RT35 [31, 34]	29-36	130–157	800	2	0.2	
Fatty acid [41]	37	216	920 (s) / 840 (l)	2.2 (s) / 2.6 (l)	0.25 (s) / 0.15 (l)	
Bio-based OM37 [42]	37	211	960 (s) / 862 (l)	2.27 (s) / 1.76 (l)	0.5 (s) / 0.44 (l)	
1-tetradecanol [40]	36-40	259.44	N.A.	N.A.	N.A.	
Paraffin [43, 44]	40	198	925 (s) / 845 (l)	2.2	0.21	
Paraffin RT42 [45]	41	175	N.A.	2	N.A.	
Paraffin RT44 [34]	41-44	255	770	2	0.2	
Paraffin C22 [28]	44	226	818 (s) / 760 (l)	2.95(s) / 2.51 (l)	N.A.	
Paraffin A44 [46, 47]	44-45.7	242-245	805	2.15	0.18	
Lauric acid [40]	44-46	228.90	N.A.	N.A.	N.A.	
Paraffin [48]	45	198	928 (s) / 832 (l)	2.11	0.2	
Paraffin [49-52]	46–48	200–220	900	2.14–2.19	0.15–0.24	
Paraffin [53, 54]	49	196	930 (s) / 830 (l)	2.1	0.21	
Paraffin RT50 [34]	50	168	780	2	0.2	
Paraffin [40]	52-54	167.27	N.A.	N.A.	N.A.	
Paraffin RT55 [45]	55	170	N.A.	2	N.A.	
Paraffin [55]	57	200–220	910 (s) / 810 (l)	2 (s) / 2.1 (l)	0.24	
Paraffin [27]	47	168	880 (s) / 760 (l)	2	0.2	CPV/T
Paraffin [56, 57]	47	266	818 (s) / 760 (l)	2.95(s) / 2.51 (l)	0.24	
Paraffin [58]	50	N.A.	900 (s) / 700(l)	2.2 (s) / 1.7 (l)	N.A.	
Paraffin RT60 [59]	55	225.2	802	2	0.2	

Paraffin [60]	56	256	N.A.	N.A.	N.A.	
Paraffin [27]	57	152	880 (s) / 780 (l)	2	0.2	
Paraffin [27]	72	182	880 (s) / 770 (l)	2	0.2	
Paraffin [27]	92	200	950 (s) / 850 (l)	2	0.2	
Inorganic						
Hydrated Salt [61]	22	215	1530	2.2	0.54	FPPV/T
Hydrated Salt (S25) [62]	25	180	1530	2.2	0.54	
Hydrated Salt (HS29) [63]	28-30	205	1600	1.44	1.09 (s) / 0.54 (l)	
$CaCl_2 \cdot 6H_2O$ [31, 64]	29.8-31	191	1710 (s) / 1560 (l)	1.4 (s) / 2.1 (l)	1.08 (s) / 0.56 (l)	
$Na_2SO_4 \cdot 10H_2O$ (70%)–$N_2O_6Zn \cdot 6H_2O$ (30%) [65]	30	241	N.A.	N.A.	N.A.	
$Na_2SO_4 \cdot 10H_2O$ [66]	32	251	1458(s) / 1485 (l)	1.76 (s) / 3.3 (l)	N.A.	
$Na_2HPO_4 \cdot 12H_2O$ [67]	37	265	1507	1.69	0.514	
$Na_3PO_4 \cdot 12H_2O$ [28]	37	280	1522	1.94 (s) / 1.69 (l)	N.A.	
NaOH (24%)–KOH (76%) [27]	147	205	2100 (s) / 2050 (l)	$0.435 + 2.451 \times 10^{-3} \times T$ (K)	0.6	CPV/T

N.A. stands for not available; s and l denote solid and liquid, respectively.

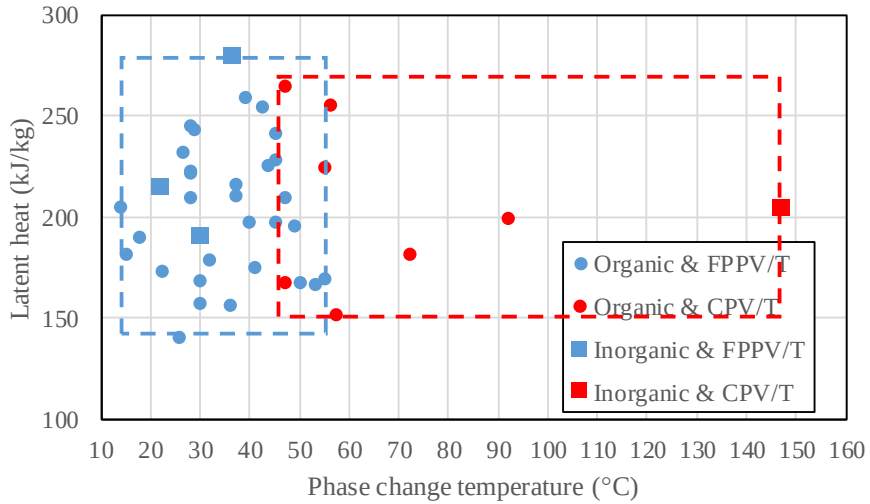

Fig. 3 Distribution of phase change temperature and latent heat of PCMs used in PV/T systems in the literature

4. Utilization of bulk PCMs in PV/T modules

This section presents the integration configurations of bulk PCMs in various PV/T modules, roles of bulk PCMs integrated into PV/T modules, influences of key parameters on the performances of PV/T modules with bulk PCMs as well as relevant heat transfer enhancement methods.

4.1 Configurations of PV/T modules integrated with bulk PCMs

Fig. 4 shows two typical integration configurations of bulk PCMs in an air-based PV/T module. A PCM layer is positioned above and below the air layer in the two configurations, respectively. The air layer is not embedded in the PCM layer. Su et al. [68] reported that the upper PCM position reduced the maximum cell temperature by 5 °C and increased the stored heat in PCM by 48% compared to the lower PCM position, while the upper PCM position enhanced the overall energy efficiency by 63%. Therefore, the configuration of the upper PCM position is preferable.

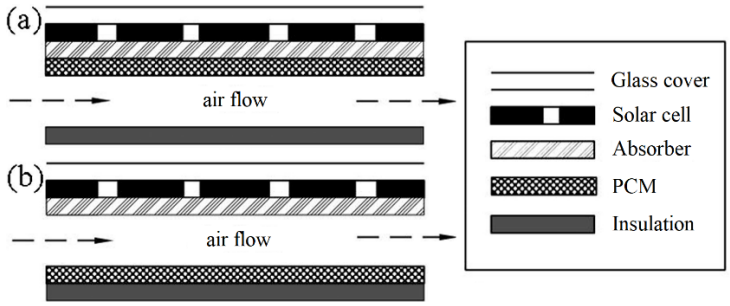

Fig. 4 Two integration configurations of PCM in an air-based PV/T module [68]

Another special integration configuration of PCM in an air-based PV/T module designed by Sudhakar et al. [63] is illustrated in Fig. 5. A cool thermal energy storage (CTES) tank containing PCM balls was installed at the upstream position of a PV/T module. The PCM balls stored the natural cold energy from the cold ambient (20–25 °C) during the night while the stored cold energy was released to cool the PV panel during the day by air flow. After a PCM with 29 °C melting point was adopted, the air temperature from the tank was maintained at around 30 °C during the day with 35 °C ambient air temperature, which effectively reduced

the panel temperature compared to the conventional case. The improvement could be more considerable for larger diurnal temperature variation. Air-based PV/T modules can be easily integrated into buildings with simple designs and minor building structure retrofitting to form BIPV/T systems. More discussions on the integration of PCMs into air-based PV/T are elucidated with BIPV/T in Section 6.

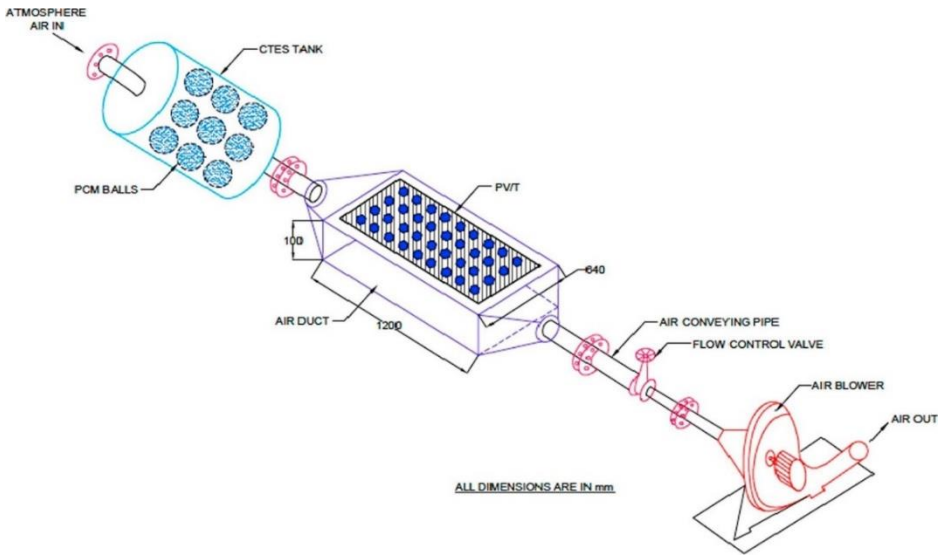

Fig. 5 Integration configuration of PCM storing natural cold in an air-based PV/T module [63]

More configurations for the integration of PCMs into water-based PV/T modules are available in the literature. Gaur et al. [42] designed a PV/T module where a PCM layer is positioned beneath the water channels as presented in Fig. 6a. The PCM layer is separated from the water channels. Salem et al. [64] proposed a novel arrangement of PCMs in a module, where the channels beneath cells are occupied by PCMs or water flow at intervals as Fig. 6b shows. Imam et al. [60] investigated a module where half of each water pipe is embedded in a PCM layer as displayed in Fig. 6c. Kazemian et al. [69] and Su et al. [70] explored a PV/T module in which each water pipe is totally embedded in the upper part (see Fig. 6d) and the centre (see Fig. 6e) of a PCM layer, respectively. There is no study on the comparison between the above different configurations**.** It is hard to determine which configuration is preferable. Nevertheless, the configuration type in Fig. 6d is the most prevalent. Since nanofluids can be

used to directly replace water, the incorporation of PCMs into nanofluid-based modules almost adopts the configuration similar to Fig. 6d [49].

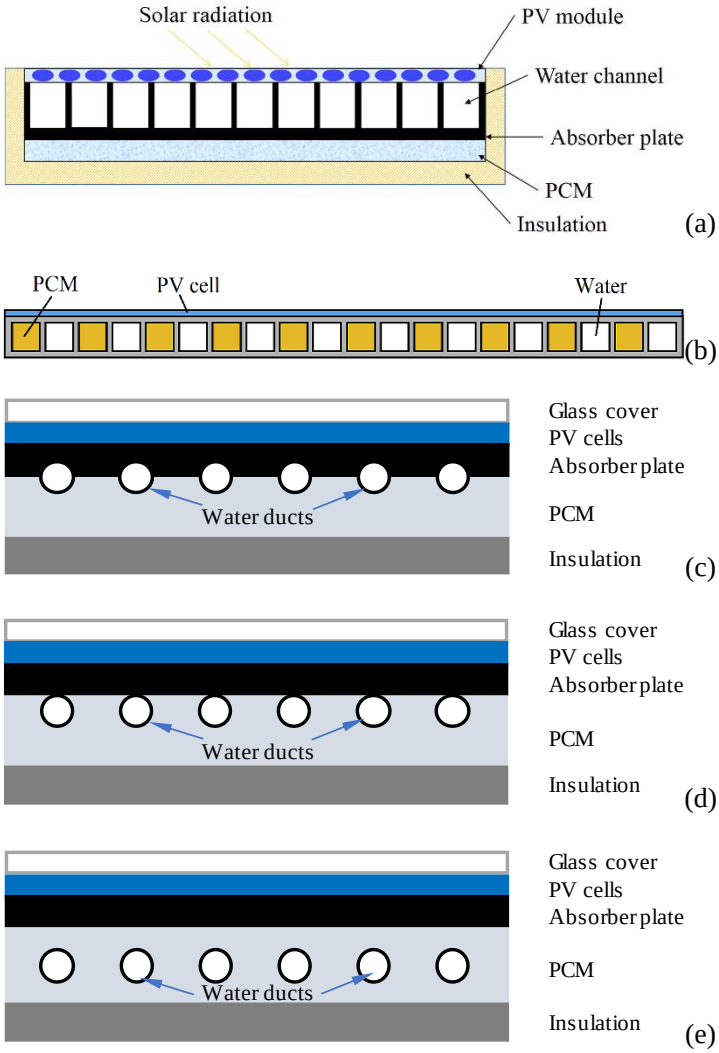

Fig. 6 Different configurations of PCMs in water-based PV/T modules: (a) the PCM layer is located beneath the water channels [42]; (b) the PCM layers are located between the water channels [64]; (c) half of each water duct is embedded in the PCM layer [60]; (d) each water duct is totally embedded in the PCM and attached on the absorber plate [69]; (e) each water duct is embedded in the PCM layer centre [70].

To fit concentrated solar radiation, a novel CPV/T module integrated with PCM is as illustrated in Fig. 7. A sphere is designed to use its upper surface to support PV cells while its inner cavity is filled with PCM to cool the cells and store thermal energy. The sphere is placed at the focus of a concentrator with an adjustable orientation. Although the design was referred to as a CPV/T module, Gürel et al. [56] did not state how to extract the heat from the PCM and

use it. A curved water pipe embedded in the PCM inside the sphere is a feasible option. Ceylan et al. [71] further placed the sphere bottom part without being covered by cells in an air channel through which the stored heat in the PCM was transferred into a drying chamber with the aid of a fan to dry product.

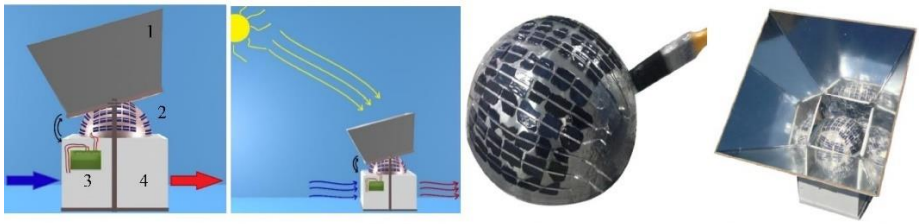

1. Concentrator, 2. The sphere filled with paraffin and covered with broken cells,
3. Charging regulator, 4. Gel accumulator and fans (in the box)

Fig. 7 A novel CPV/T module integrated with PCM [71]

4.2 Roles of bulk PCMs integrated into PV/T modules

The bulk PCMs integrated into PV/T modules can play different roles according to various design purposes, which mainly include PV cell cooling, anti-freezing, thermal efficiency improvement and heat supply regulation.

4.2.1 PV cell cooling

Based on the absorption of latent heat during the melting, PCMs only served as an auxiliary cooling medium to reduce the cell temperature in several studies. Fayaz et al. [47] demonstrated that adding PCM with a configuration similar to Fig. 6a reduced the cell temperature by 6.3 °C and therefore increased the electrical efficiency by 0.31%, but it decreased the thermal efficiency by 6.4%. AL-Musawi et al. [72] and Preet et al. [35] also demonstrated similar results for PV/T-PCM modules with the configurations in Figs. 6d and 6e, respectively. This is because the PCM absorbed a portion of the heat to cool the cell but subsequently the absorbed heat was dissipated into the environment without being applied as useful energy (i.e. wasted). Furthermore, the PV panel had a more uniform temperature

distribution after adding PCM because the PCM layer covered the whole rear surface of the absorber plate to absorb heat [69].

4.2.2 Anti-freezing

The heat stored in PCM during the daytime can be utilized during the night. Yuan et al. [73] proposed to release the heat stored in PCM during the night to prevent a water-based PV/T module with a configuration similar to Fig. 6a from freezing in winter. Although the module with PCM proposed in their work was not superior to the module without PCM in the thermal efficiency, the module still had a temperature of > 0 °C at night in cold winter with the aid of PCM and thus avoided freezing, which is an advantage of the proposed module with PCM.

4.2.3 Thermal efficiency improvement

To enhance thermal efficiency, the stored heat in PCMs was utilized as useful energy output in more studies. Kazemian et al. [69] stated that the thermal efficiency of a PV/T-PCM module with the configuration in Fig. 6d was 34.2% as excluding stored heat in PCM and 57.3% as including stored heat, while that of a PV/T module was 43.9% (see Fig. 8). Therefore, the heat stored in PCM should be made full use of to ensure the considerable superiority of using PCM in improving the thermal efficiency. Su et al. [68] also demonstrated that the thermal efficiency of a PV/T-PCM module with the configuration in Fig. 4a was much higher than that of a PV/T module as counting in the stored heat in PCM. Besides the heat storage function of PCM, the thermal efficiency improvement should also be attributed to the decreased module temperature, which leads to the reduction of heat loss through surrounding air convection and radiation. Along with the increased electrical efficiency, the average overall energy efficiency was therefore increased by 10.7% [68] and 14.1% [69] after adding PCM.

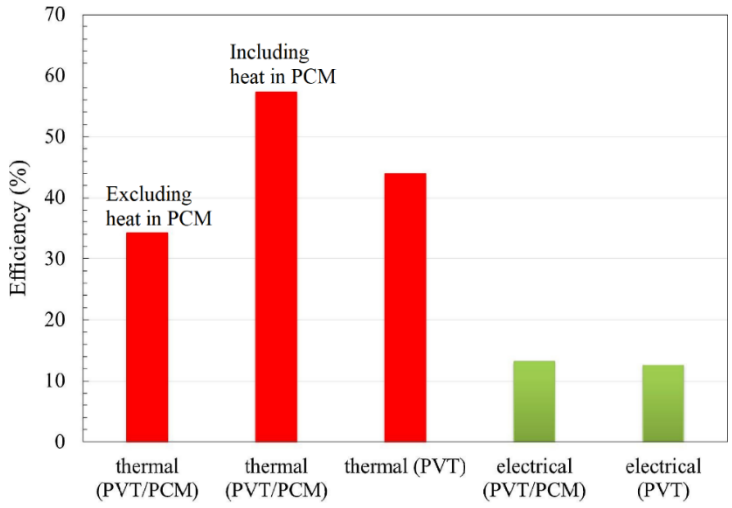

Fig. 8 Comparison of energy efficiencies between PV/T and PV/T-PCM modules [69]

4.2.4 Heat supply regulation

Besides improving the energy efficiency, the PCM heat storage also increases the duration and flexibility of thermal energy supply (e.g. hot water supply) of PV/T modules. Browne et al. [74] manifested that the duration of supplying warm water nearly doubled after PCM heat storage was integrated with the configuration in Fig. 6d. Su et al. [70] assumed that the water was pumped into module pipes only after 17:00 to extract heat in the module with the configuration in Fig. 6e. In such an operation mode, the daily thermal energy output increased by 3.7 MJ after adding PCM while the maximum cell temperature dropped by 19 °C. Gaur et al. [42] stated that the melted PCM in the module with the configuration in Fig. 6a served as a heat source during the night to provide hot water until the next morning, of which the temperature reached 34.78 °C even in winter, while it was only 14.98 °C for the case without PCM. As shown in Fig. 9, the module without PCM produced more thermal power during the daytime than one with PCM, but it was reversed because the heat stored in PCM was released when solar radiation was low in the evening or absent at night. The daily thermal energy output increased by 64% for winter and 41.7% for summer after adding PCM.

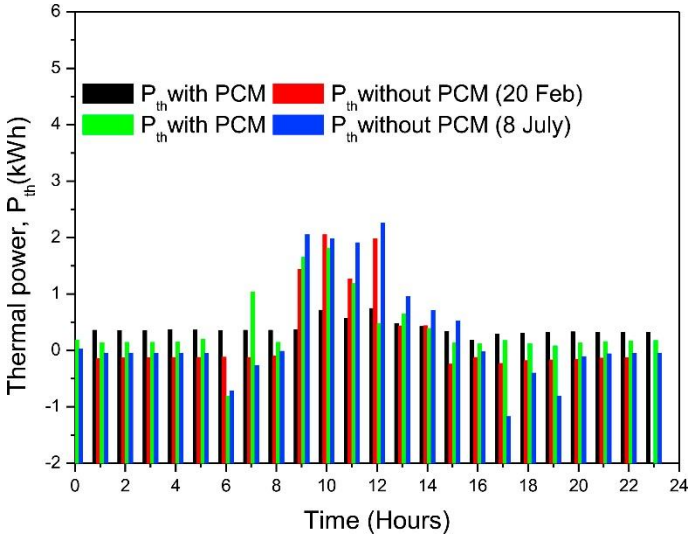

Fig. 9 Hourly thermal power generated by PV/T modules in winter (20 Feb) and summer (8 July) [42]

4.3 Effects of key parameters on PV/T modules with bulk PCMs

The performances of PV/T modules integrated with bulk PCMs can be affected by some key parameters, such as thermophysical properties and mass of adopted PCMs, operation parameters of working fluids and environmental conditions, which have been widely investigated experimentally or numerically.

4.3.1 Effects of PCM melting temperature

As presented in Fig. 10, there exists an optimal PCM melting point T_m for the PV output of a PV/T-PCM module, while the PV output could be reduced by almost 2% if a too high T_m was selected; An optimal T_m was achieved if the melting period of PCM was approximately equal to its solidification period; If T_m was too high or too low, the melting/solidification was possibly incomplete; The optimal T_m was determined by the environmental conditions. For instance, the optimal T_m was 28 °C for the air temperature range of 10–20 °C, while it was 32 °C for the air temperature range of 20–30 °C [33]. Therefore, an optimal T_m based on a constant climate was hard to meet the climate changes throughout the year and T_m should be selected with compromise based on the climate of the whole year.

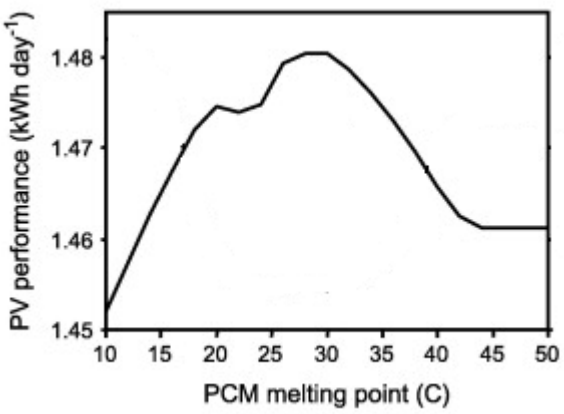

Fig. 10 PV output variation with PCM melting point [33]

AL-Musawi et al. [72] declared that the augment of T_m in the range of 31–54 °C elevated cell temperature and decreased electrical efficiency, while its thermal efficiency was improved. Kazemian et al. [69] stated that both the cell temperature and the obtained water temperature rose as T_m increased from 40 °C to 65 °C, whereas the melted PCM ratio was dramatically reduced. Thus, the resulting electrical and thermal efficiencies were reduced. As Fig. 11 shows, the lowest cell temperature was achieved at T_m = 30 °C without warm water output, the warmest water was achieved at T_m = 60 °C and the longest warm water supply duration was achieved at T_m = 40 °C [70]. Since it maximized the thermal energy output, the case of T_m = 40 °C generated maximum overall energy output.

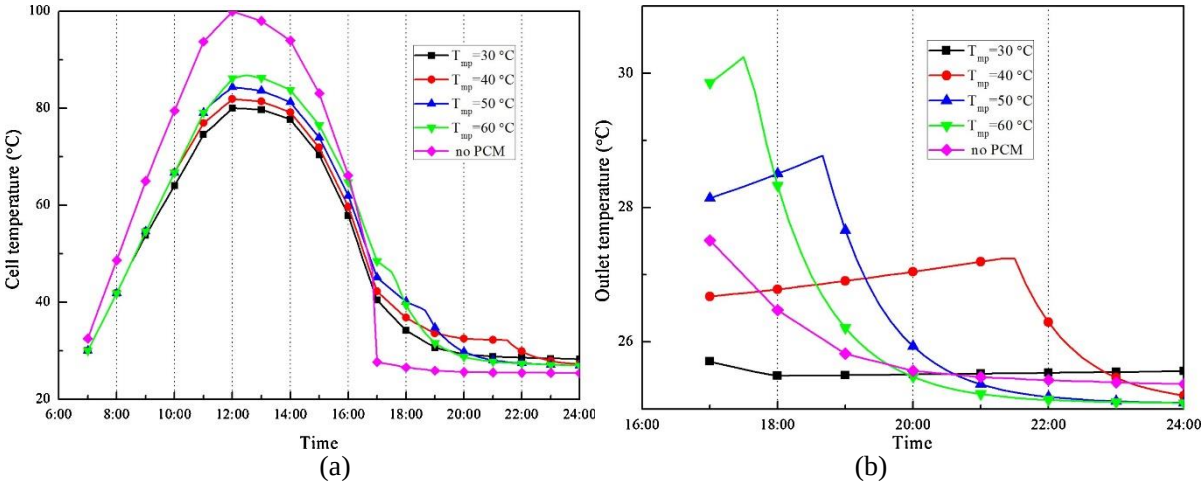

Fig. 11 The hourly variation of (a) PV cell temperature and (b) outlet water temperature for various PCM melting points [70]

T_m also determines the ability of PCM to prevent water in the PV/T module from freezing at night of winter. Yuan et al. [73] stated that the PCM of T_m = 15 °C failed to prevent the water from freezing after 3:00 in the night while the PCM of T_m = 5 °C succeeded in keeping the water above 0 °C for the whole night. This should be attributed to a smaller temperature difference between the ambient and PCM for T_m = 5 °C, which lengthened the solidification process of PCM to release heat throughout the whole night and prevent the water from freezing. However, the PCM of T_m = 5 °C can hardly meet the requirement of reducing the cell temperature in the daytime because the low T_m made it to be melted in a short period and unable to absorb more heat. Therefore, a possible solution to meet both the requirements is to adopt a combination of PCM layers with different melting points.

4.3.2 Effects of PCM latent heat

With increasing PCM latent heat by 2.8 times, the cell temperature reduces by 3.9% and therefore the electrical efficiency increased by 0.48%; although the melted PCM ratio and the water outlet temperature were reduced by 29.87 % and 0.4% respectively, the thermal efficiency was enhanced by 2.31% [69]. It implies that such a dramatic rise in PCM latent heat brought very little effect on the thermal and electrical efficiencies.

4.3.3 Effects of PCM thermal conductivity

As PCM thermal conductivity was enhanced by 5 times, the cell temperature decreased by 3.3 °C, while the water outlet temperature was nearly kept constant. Consequently, the electrical and thermal efficiencies were enhanced by 1.34% and 6.59%, respectively [69]. The PV output was improved by 3% when PCM thermal conductivity was increased by 10 times [33]. These studies highlight the requirement of adopting metal fins, nanoparticles or encapsulation for PCM, which are elaborated in Section 4.4. Nevertheless, a 10 times enhancement of thermal conductivity is hard to achieve unless new PCMs were developed.

4.3.4 Effects of PCM thickness or mass

With the increase of PCM thickness, the cell temperature first decreased and then increased [68] or kept constant [33]. The difference is caused by the relative position between the fluid channel and the PCM layer. Nevertheless, there existed an optimal PCM thickness (3 cm) to obtain the lowest cell temperature at the lowest cost for both cases, which indicated the maximum melting depth in the PCM layer. In some cases, an excessively small PCM thickness (such as 2 cm) was ineffective to reduce the cell temperature as shown in Fig. 12a due to the heat return after overheating of PCM [68]. Although unduly increasing the PCM thickness was not helpful in reducing the cell temperature, it was beneficial for preventing the water from freezing if the module size is not limited [73].

For maximizing the overall energy output, there also existed an optimal PCM thickness but it varied with the PCM melting point as Fig. 12b presents [70]. Under realistic climate conditions, the water outlet temperature decreased with an increase in the PCM mass during the daytime while it first increased and then decreased during the night [42]. There exists an optimal PCM mass to obtain the highest water outlet temperature in the night. This resulted from the compromise between thermal resistance and latent heat capacity which both increased with the PCM mass.

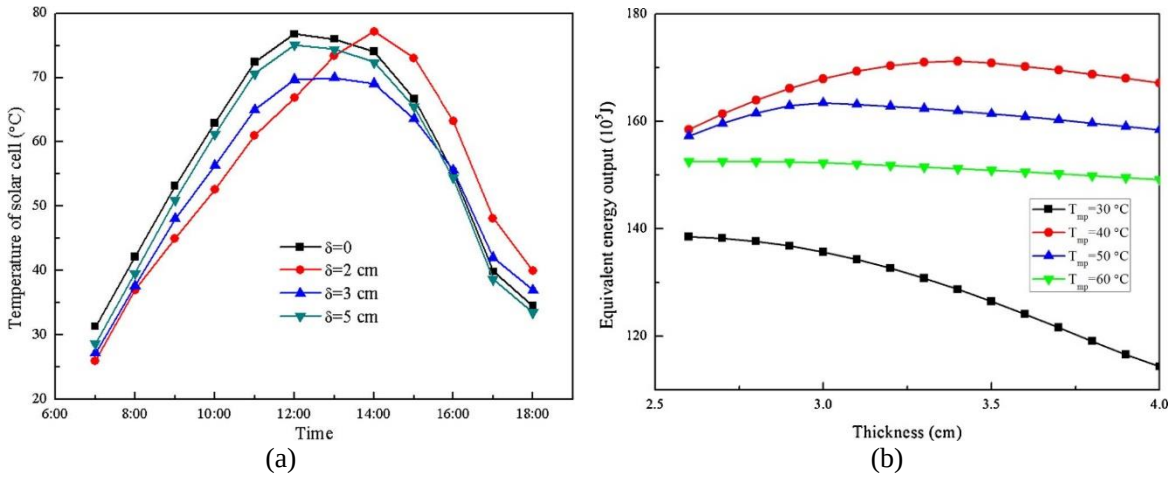

(a) (b)

Fig. 12 Effects of PCM thickness: (a) on cell temperature [68] and (b) on overall energy output [70]

4.3.5 Effects of flow rate of working fluids

Kazemian et al. [69] stated that the melted PCM ratio was reduced as the water flow rate increased and therefore the role of PCM was weakened. Malvi et al. [33] showed that the PV output was enhanced with increasing water flow rate. However, the outlet water temperature was reduced simultaneously, which is undesired for hot water supply. Preet et al. [35] demonstrated that the electrical efficiency increased with the water flow rate. Fayaz et al. [47] verified that the electrical and thermal efficiencies were both enlarged with the water flow rate. Hossain et al. [40] found that the variation curve of thermal efficiency versus the water flow rate exhibits a bell-like shape. It was advised to select a flow rate between 1 and 2 L/min to obtain an acceptable water temperature without obviously reducing thermal efficiency. They further stated that a lower water flow rate should be adopted to substantially reduce the irreversibility for obtaining higher overall exergy efficiency.

4.3.6 Effects of environmental conditions

The environmental conditions mainly include solar irradiation and environmental temperature. Some studies have been devoted to the effects of solar radiation alone on PCM melting inside PV/T-PCM modules and module performances. Kazemian et al. [69] indicated that as solar irradiation increased, PCM melting was notably speeded up. Fayaz et al. [46] showed that with increasing solar irradiation both the thermal and electrical efficiencies were decreased, although both the thermal and electrical outputs were augmented. The reason is as follows: under stronger irradiation, heat generated in PV/T modules is unable to be efficiently absorbed by the PCM and water, and thus the cell temperature increases and more heat is discharged to the surroundings through thermal radiation and ambient air convection.

The ambient temperature usually changes along with the solar irradiation through one day, one month or one year. Kazemian et al. [75] allowed for the effects of the variations of both ambient temperature and solar irradiation hourly, daily and monthly. When T_m = 40 °C, no PCM melting process occurred from Nov. to Mar., which implied that the PCM did not work

due to the low ambient temperature and solar irradiation. The highest overall energy output and efficiency were achieved in July with the largest operating duration, whilst July has virtually the lowest electrical efficiency and overall exergy efficiency as Fig. 13 shows.

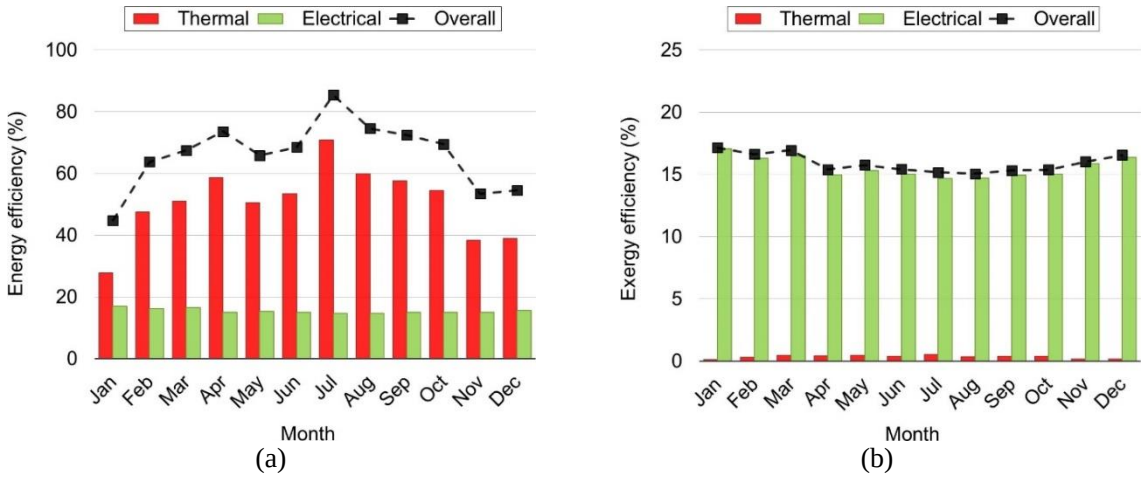

Fig. 13 Monthly average efficiencies of a PV/T-PCM module: (a) energy; and (b) exergy [75]

4.4 Heat transfer enhancement methods for PV/T modules with bulk PCMs

There are a variety of heat transfer enhancement methods for PV/T modules integrated with bulk PCMs, such as adding nanoparticles into the working fluid or PCM, inserting metal fins into PCM, embedding PCM into metal foam, and encapsulating PCM.

4.4.1 Nanoparticles

It has been proven that adding nanoparticles into a carrier fluid (such as water) to form nanofluids as the working fluid of PV/T modules can achieve heat transfer enhancement and effectively elevate module efficiency [76, 77]. More studies on the utilization of nanofluids in PV/T modules can be found in several review papers [78, 79]. This paper merely involves studies on the usage of nanofluids in PV/T-PCM modules. Sardarabadi et al. [49] demonstrated that adding 0.2wt % ZnO nanoparticles into the water as the working fluid increased the outputs of both electrical and thermal power and hence elevated the daily average overall exergy efficiency from 13.17% to 13.42%. Hosseinzadeh et al. [51] stated an overall exergy efficiency of 13.61% for the same ZnO/water nanofluid-based module under a similar climate condition.

Abdelrazik et al. [80] introduced a silver/water nanofluid for optical filtration into a graphene/water nanofluid-based module through an extra flow channel, which increased the overall energy efficiency from 70.96% to 90.25%. Manigandan et al. [81] found that CuO/water nanofluid was superior to ZnO/water nanofluid both in thermal and electrical power outputs. Salari et al. [82] demonstrated that the addition of multi-walled carbon nanotubes (MWCNT) in water gave rise to a higher improvement in the overall energy efficiency compared to MgO nanoparticles. Even so, MgO nanoparticles were viewed as a more suitable option since they had a lower cost than MWCNT. Besides adding nanoparticles into the working fluid, inserting nanoparticles into PCM is another option to enhance heat transfer to improve PV/T-PCM module performance. Ergün et al. [57] used 5 wt% Al_2O_3 nanoparticles into PCM paraffin-wax, increasing the average exergy efficiency from 9.2% to 10%. Salem et al. [64] verified that the module performance increased with the concentration of Al_2O_3 nanoparticles in PCM. To be more specific, the average exergy efficiency rose from 13.1% to 13.8% as the Al_2O_3 concentration was increased from 0.25 wt% to 1 wt%. Abdelrazik et al. [31] also added graphene nanoplatelets in PCM to improve the electrical and thermal efficiencies.

Obviously, nanoparticles can be used both in the working fluid and PCM. Al-Waeli et al. [53] added SiC nanoparticles both in the working fluid and paraffin-PCM for a water-based PV/T-PCM module to achieve larger thermal conductivities and therefore higher efficiency. Fig. 14 displays microscopic morphologies of SiC nanoparticles with a size range of 40–60 nm as well as that in Paraffin. The maximum electrical efficiency grew from 12.32% to 13.70% while the maximum thermal one rose from 50.5% to 72% after utilization of 0.1 wt% SiC nanoparticles. They also developed artificial neural network (ANN) models [83] and linear prediction models [48] to precisely forecast the performances of nanoparticles-enhanced PV/T-PCM modules in real climate conditions. Their further economic evaluation indicated that the

annual energy productivity of the proposed module was 230.73 while that of the case without nanoparticles was only 164.97 [43]. Sarafraz et al. [84] identified the effect of MWCNT added in both the PCM and the working fluid, where 0.2 wt% MWCNT achieved larger thermal and electrical power outputs compared to 0.1 wt% and 0.3 wt%.

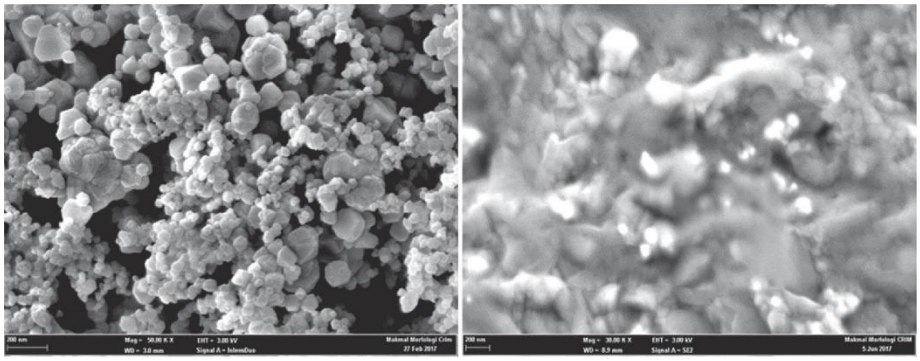

(a) (b)

Fig. 14 Morphologies of SiC nanoparticles (a) alone and (b) in Paraffin [53]

4.4.2 Fins

Lots of studies demonstrated that metal fins inserted into PCM enhanced heat transfer and therefore helped to limit temperature rise and improve temperature distribution uniformity for PV-PCM modules without working fluids or thermal utilization [85]. However, the insertion of metal fins increased the system weight or shortened the duration of effective thermal regulation because the mass of light PCM was reduced [86]. Nevertheless, metal fins were still applied in PV/T-PCM modules. Preet et al. [35] inserted aluminum fins into PCM between water tubes as illustrated in Fig. 15, aiming to enhance heat transfer. Although such a module obtained higher electrical and thermal efficiencies, the effects of the metal fins were not elucidated.

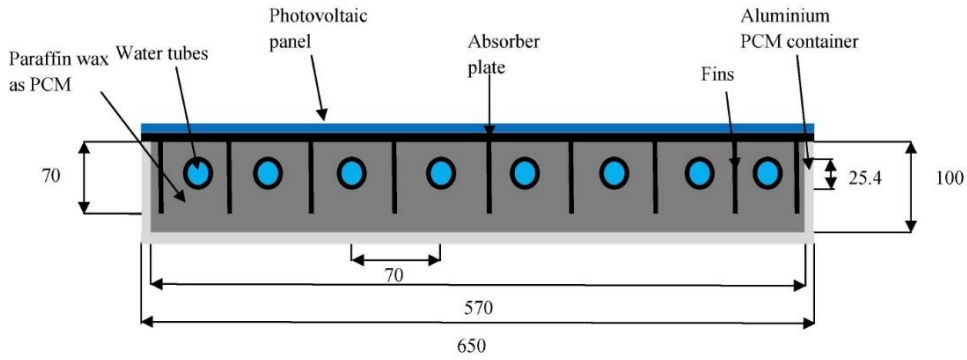

Fig. 15 A typical PV/T-PCM module with fins [35]

4.4.3 Macro-encapsulation

Encapsulation of PCM is a process of putting PCM into a sealed container by physical or chemical approaches, such as capsule, ball, rectangular box or bags [87]. Besides the purpose of holding the PCM and isolating it from the surroundings to prevent leakage and corrosion, encapsulation also is expected to reduce PCM reaction with the surrounding, improve mechanical and thermal stability, make frequent phase change flexible, increase heat transfer rate [88]. According to the size, the encapsulation can be classified into microencapsulation (<1 mm) and macro-encapsulation (>1 mm). In view of the distinct characteristics of microencapsulated PCM in thermophysical properties and operation, the studies on microencapsulated PCM in PV/T modules will be discussed in Section 5. This subsection merely involves the macro-encapsulation of PCM. Modjinou et al. [29] and Fayaz et al. [46] adopted aluminum-coated PCM panels and PCM bags as presented in Figs. 16a and 16b to elevate the performances of PV/T modules, respectively. To avoid the burning of a solar-tracking concentrated PV/T module, Su et al. [58] encapsulated PCM into spheres to enhance thermal conduction and then immersed the spheres in a water tank installed on the rear surface of the PV panel as illustrated in Fig. 16c. Their results demonstrated that this design was effective for improving system performances.

Fig. 16 Macro-encapsulated PCM: (a) Aluminium coated PCM panels [29]; (b) PCM bags [46]; and (c) PCM balls [58]

4.4.4 Metal foam

In virtue of the advantages including large porosity for taking in PCMs [89], good thermal conductive ligaments for heat transport [90], high specific surface area for heat exchange [91], open-cell metal foam are regarded as a competitive substance in enhancing heat transfer of PCMs by embedding PCMs into it, which has been verified by plenty of studies [92, 93]. Copper foam as shown in Fig.17a is a common metal foam, which has a pore density of 10 pores per inch and a porosity of 0.96. A vacuum environment, such as 94 Pa, was required to ensure the copper foam was totally infiltrated by liquid paraffin PCM to form PCM/foam composite (see Fig. 17b) [94]. Such a copper foam was applied to promote the efficiencies of a PV/T-PCM module by Mousavi et al. [28]. Their simulations identified an enhancement of 7% in the overall exergy efficiency after adopting the copper foam.

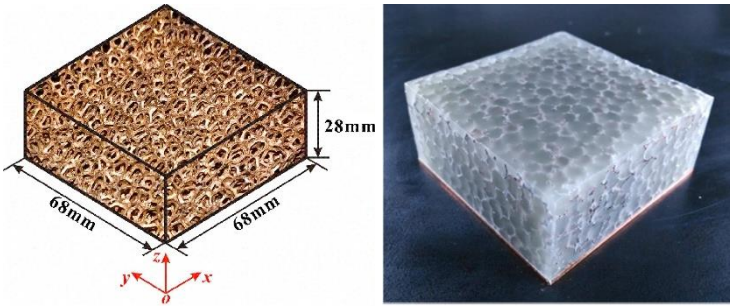

(a) (b)

Fig. 17 A cuboid copper foam before (a) and after (b) being infiltrated by paraffin PCM [94]

4.5 Economic analysis for PV/T modules with bulk PCMs

The exergo-economic analysis conducted by Maatallah et al [55] demonstrated that compared to conventional PV modules, the electricity generation cost and energy payback period of a water-based PV/T-PCM module were decreased by about 0.05–0.1 €/kWh and 0.76 year, respectively, due to the increase in electrical efficiency and the thermal usage, although its uniform annual cost was increased by about 1–4.5 € owing to more material and maintenance requirements. Hossain et al. [40] stated that the payback period of a water-based PV/T-PCM module was about 4 years, which was about 2 years less than that of a conventional PV panel, although the annual cost of the former was much higher than that of the latter, which were US$ 434.35 and US$ 133.82 for the first 5 years, respectively. Al-Waeli et al. [43] detailedly compared the life cycle cost, capital cost, maintenance cost, replacement cost and annual energy productivity among three PV/T modules using water, nanofluid or nanofluid/nano-PCM. They concluded that the nanofluid-based PV/T-PCM module exhibited an energy cost of 0.112 USD/kWh and a payback period of 4.4–5.3 years, whereas the corresponding data for other PV/T modules were lacking for further comparison. The above studies indicated that PV/T-PCM modules were economically feasible in the long term. However, these comparisons in the above studies cannot completely reveal the cost and benefit caused by the integration of PCM in PV/T modules because they did not eliminate the role of

water or nanofluid. More detailed economic analyses are required to clearly compare the cost-benefit advantage between PV/T modules with and without PCM.

5. Utilization of MPCM slurry in PV/T modules

As mentioned in Section 4.4.3, PCM can be microencapsulated to form a shell/core structure to avoid corrosion and leakage, improve heat transfer performance, etc. There are many methods to synthesize the microencapsulated PCM (MPCM), such as in-situ suspension, interfacial and emulsion polymerization, etc. [95]. The microscopic image of MPCM (i.e. PCM microcapsule) is shown in Fig. 18a [96]. The MPCM usually suffers from shell cracking or buckling which will affect its stability and effectiveness. Yu et al. [97, 98] developed a thermo-mechanical coupled model to determine the critical conditions of avoiding cracking or buckling in shell thickness and material selection. Uniformly dispersing MPCM particles into a carrier fluid (e.g. water) can form MPCM slurry when the MPCM particles are small enough (<100 μm in diameter generally) to be suspended in the carrier liquid as Fig. 18b shows. Phase change may take place in MPCM slurry during heating or cooling but only the PCM core changes between solid and liquid states [99]. The MPCM slurry, therefore, has a large apparent specific heat (including PCM latent heat) near the melting point and good fluidity to be transported by pumps. Also, the metal shell adopted in some cases, the micro-convection caused by MPCM motion, and the interactions of particle-particle, particle-fluid and particle-wall are helpful to heat transfer enhancement. As a result, the MPCM slurry can act as both the heat storage medium and heat transfer fluid [100, 101]. Much work has been conducted on thermal properties and various applications of MPCM slurries [102]. MPCM slurry is a promising alternative as the working fluid in PV/T modules.

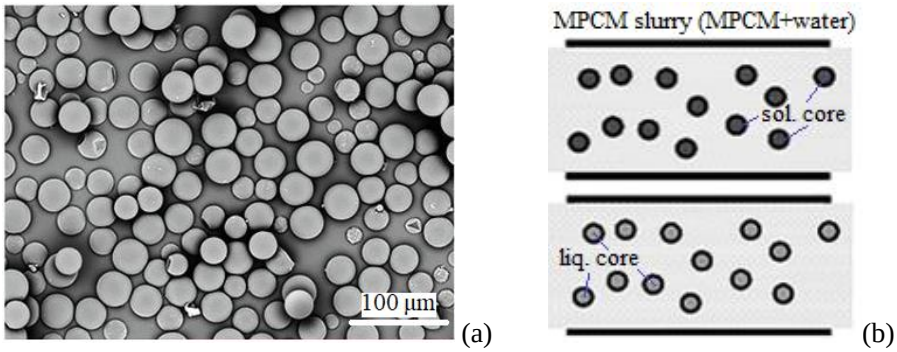

Fig. 18 MPCM particles (a) [96] and MPCM slurry with phase change under heating or cooling (b)

5.1 Performance comparison between PV/T with MPCM slurry and water

The comparisons in this subsection are carried out under the optimal configurations of MPCM slurry reported in each paper, such as MPCM concentration, melting point and flow rate. For a dual-channel PV/T module (see Fig. 19a), Liu et al. [103] stated that although the output temperature of the slurry case was much smaller caused by the latent heat, the slurry case still had up to 1.8% higher thermal efficiency compared to the water case during the whole day. The slurry case also had a slightly lower cell temperature and thus a slightly higher electrical efficiency. Although more pump power was consumed in the slurry case owing to a higher viscosity, the slurry case had a higher net efficiency. Jia et al. [104] concluded similar performance improvements as MPCM slurry was applied to replace water.

For a CPV/T module (see Fig. 19b), Liu et al. [105] indicated that the cell temperature was reduced by up to 5 °C and the output fluid temperature variation was reduced from 12 °C to 7 °C after the MPCM slurry was adopted. Also, the thermal and electrical efficiencies both increased and therefore the overall energy efficiency achieved an increase of 3.5%–6.6%.

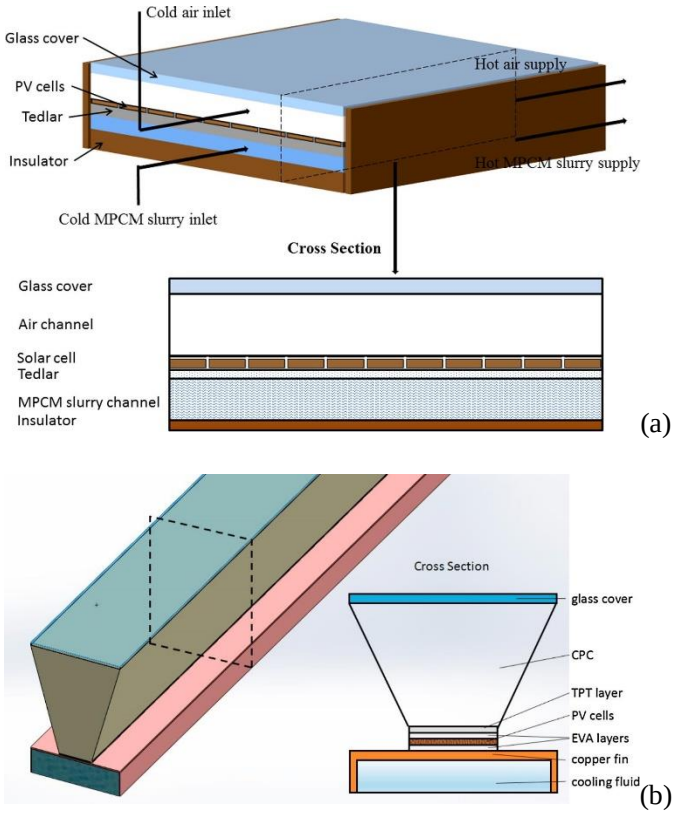

Fig. 19 PV/T with MPCM slurry: (a) dual-channel [103] and (b) parabolic concentrating [105]

For a module as shown in Fig. 6d, Yu et al. [106] revealed that when the MPCM slurry with $T_m = 27$ °C was applied, the average cell temperature decreased by up to 6.2 °C with more uniform temperature distribution and the primary-energy saving efficiency increased by up to 7%, whereas the exergy efficiency became smaller than the water case. Further, when the MPCM slurry with $T_m = 47$ °C was applied, the primary-energy saving efficiency and exergy efficiency were both enhanced with an increase of 3% and 0.4% respectively, while the cell temperature decreased by 2.5 °C.

For a module with wavy tubes, Eisapour et al. [107] reported after applying MPCM slurry to replace water, the electrical and thermal efficiencies increased by 0.54% and 4.69%, respectively, whereas the overall exergy efficiency decreased instead. They also added Ag nanoparticles into MPCM slurry to form MPCM-nano slurry to further improve the module performance. Compared to the water case, the use of MPCM-nano slurry increased the

electrical efficiency by 0.6% and the thermal efficiency by 8.58% without reducing the overall exergy efficiency.

Some PCM particles without microencapsulation can be steadily dispersed in a carrier fluid without sediment and stratification, such as alkyl hydrocarbon PCM slurry. For a module integrated with a heat pipe, Chen et al. [108] reported that the daily average electrical and thermal efficiencies increased by 0.8% and 5%, respectively, after applying the PCM slurry to replace water to absorb heat from the heat pipe condensation section.

5.2 Effects of key parameters on PV/T modules with MPCM slurry

The key parameters of MPCM slurry include MPCM concentration, melting point, latent heat, slurry flow rate, and Reynolds number, etc., which have significant effects on PV/T module performances. The effects of the key parameters have been studied by several researchers which are gathered in Table 4.

Table 4 Studies on the effects of key parameters of MPCM slurry on PV/T modules.

References	Key parameters of MPCM slurry studied	Approach
Qiu et al. [26]	MPCM concentration, Reynolds number	Numerical (1-D)
Qiu et al. [109]	MPCM concentration, Reynolds number	Experimental
Liu et al. [103]	Mass flow rate, MPCM concentration, Latent heat, MPCM thermal conductivity	Numerical (2-D)
Jia et al. [104]	Mass flow rate, MPCM concentration	Numerical (2-D)
Liu et al. [105]	Mass flow rate	Numerical (3-D)
Yu et al. [106]	Inlet fluid velocity, MPCM concentration, Melting temperature	Numerical (3-D)
Eisapour et al. [107]	MPCM concentration	Numerical (3-D)

1-D denotes one-dimensional.

5.2.1 Effects of MPCM concentration. Qiu et al. [26] stated that under a constant flow velocity, increasing MPCM concentration can result in flow transition from turbulent to

laminar because of decreasing Reynolds number, which would result in obvious heat transfer deterioration and severely decreased energy performance. The increase of MPCM concentration without flow transition slightly enhanced the thermal and electrical efficiencies. At a constant Reynolds number, the cell temperature was decreased and all the electrical thermal, and overall efficiencies were enhanced with increasing MPCM concentration, whereas the net efficiency first grew and then dropped because the pressure loss (i.e. pump power consumption) notably increased. The concentration corresponding to the net efficiency peak value decreased at a higher Reynolds number. Their experiments further verified the changing trend of net efficiency [109]. Liu et al. [103] and Jia et al. [104] showed a monotonously increasing tendency for all efficiencies including the net efficiency with increasing MPCM concentration although the growth slowed down. Yu et al. [106] reported that a larger enhancement for the primary-energy saving efficiency was obtained at a smaller fluid velocity by increasing MPCM concentration, while the largest enhancement for the overall exergy efficiency occurred at a fluid velocity of 0.095 m/s. Eisapour et al. [107] claimed that increasing the MPCM concentration resulted in enhanced thermal and electrical efficiencies whereas the overall exergy efficiency was slightly decreased.

5.2.2 Effects of MPCM melting point. Yu et al. [106] adopted three MPCM melting points (T_m= 27 °C, 37 °C and 47 °C) to assess the impacts of T_m on PV/T module performances. With a decrease of T_m, both all the energy efficiencies were improved but the improvement from 47 °C to 37 °C diminished or even vanished at a higher fluid velocity. The thermal exergy is determined by the amount and the temperature of absorbed heat. The thermal exergy and overall exergy efficiency for T_m=27 °C were the lowest since most heat was absorbed as the latent heat at 27 °C, while the highest values shifted from the case of T_m=47 °C to that of T_m=37 °C as the inlet velocity increased.

5.2.3 Effects of MPCM latent heat and thermal conductivity. Liu et al. [103] identified that both a higher latent heat and a higher thermal conductivity were helpful for reducing cell temperature and improving thermal, electrical and net efficiencies. Higher latent heat can only be obtained by selecting proper PCMs or decreasing the shell thickness of microcapsules. All the MPCM particles adopted by the studies as listed in Table 4 have a small thermal conductivity of < 0.8 W/m·K, which can be enhanced by adopting metal shells or inserting nanoparticles in the shell or core.

5.2.4 Effects of Reynolds number (mass flow rate or fluid velocity). Qiu et al. [26] demonstrated that increasing Reynolds number enhanced the thermal and electrical efficiencies while the enhancement effect reduced at a higher MPCM concentration. The net efficiency increased with Reynolds number at a small MPCM concentration (e.g. 5%) whereas the tendency was reversed at a large concentration (e.g. 20%). Their experiments indicated that the net efficiency first increased and then decreased with increasing Reynolds number at 10% MPCM concentration [109]. Liu et al. [103] stated that as the mass flow rate increased both the thermal and net efficiencies showed ‘‘*N*’’-shape changing trends, whilst the electrical efficiency monotonously increased. Jia et al. [104], Liu et al. [105], and Yu et al. [106] all presented a monotonously increasing tendency for thermal and electrical efficiencies with an increase of the inlet fluid velocity or mass flow rate, while the exergy efficiency diminished.

6. Development of BIPV/T-PCM systems

Nearly one-third of the worldwide energy consumption is devoted to the creation of an artificial environment in buildings [110], which urges the development of net-zero energy buildings. Building-integrated PV/T (BIPV/T) is a promising and sustainable solution that has drawn considerable attention [111]. BIPV/T systems are attached to building envelopes to supply electrical and thermal energy on site or improve building energy efficiency. In recent

years, increasing studies have been conducted on the performances of BIPV/T coupled with PCM (BIPV/T-PCM). The integration of PCM is expected to better manage the PV panel temperature or building energy demand. Since BIPV/T is generally installed on the roof or the façade, this sub-section is organized from the two installation categories.

6.1 BIPV/T on the roof

A water-based BIPV/T on the roof integrated with an independent PCM storage unit (see Fig. 20) was proposed for space heating by Yin et al. [112]. In the water circulation, the heat produced by the PV/T module was gathered via the circulated water to limit the cell temperature rise, and released in the floor radiant unit for day-time heating or extracted into the PCM unit for night-time heating to ensure indoor thermal comfortableness throughout the day. The PCM heat storage solved the mismatch between supply and demand of heat and simultaneously precool the circulated water for maintaining the continuous operation. However, no data was provided in their work to demonstrate the role of PCM in improving the energy conversion efficiency, energy-saving performance and indoor thermal comfort. Lari et al. [36] claimed that a similar PV/T-PCM system covered 27.3% of the annual thermal load and 77% of the annual electrical load in a residential building.

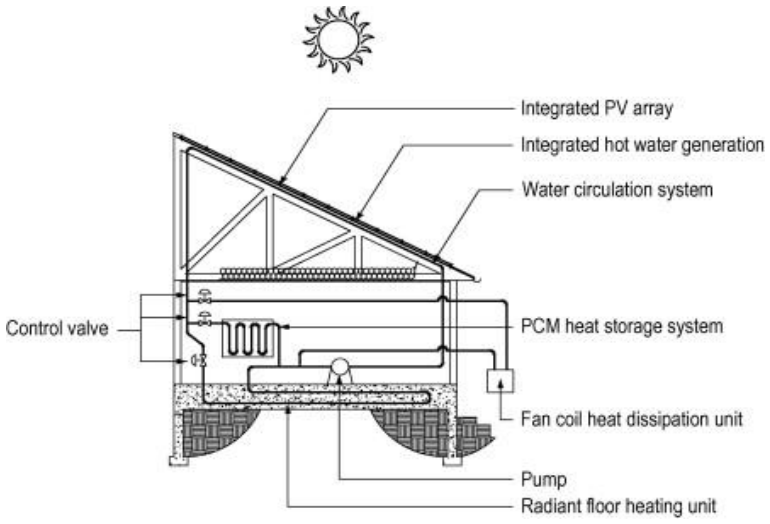

Fig. 20 Schematic of a water-based BIPV/T on the roof with PCM heat storage [112]

An air-based BIPV/T on the roof integrated with an independent PCM storage unit was designed to assist an HVAC system by Fiorentini et al. [61]. A cost function C as expressed in Eq. (1) was introduced to indicate the stored heat P_{th} in the PCM unit with considering electrical power $P_{e,\ cons}$ consumed by the fan for transporting the air and electrical generation increment $\Delta P_{e,\ gen}$ caused by the air cooling under the PCM charging mode. For increasing the importance of electrical energy, a weighting factor α_c was adopted in this equation.

$$C = P_{th} + \alpha_c(\Delta P_{e,\ gen} - P_{e,\ cons}). \qquad (1)$$

Fig. 21 implies that the cost function can be maximized by adjusting the air flow rate to optimize the PCM charging model. A similar cost function was also introduced to optimize the PCM discharging model. They further scheduled a dynamic operation scheme to achieve decent indoor thermal comfort with optimized overall energy efficiency [113]. Ren et al. [114] adopted Taguchi method for a similar BIPV/T-PCM system to explore the stored useful energy in the PCM unit, which proved to be mainly affected by the PCM type and air flow rate.

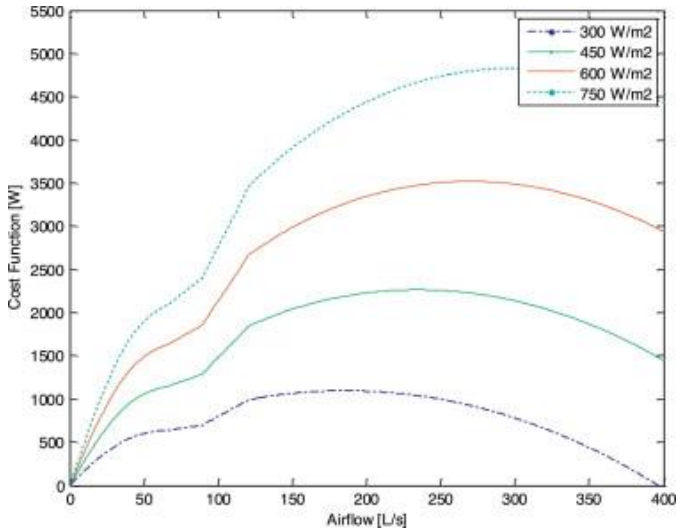

Fig. 21 Variations of the cost function with air flow rate under different radiation intensities [61]

Besides as an independent storage unit, the PCM can also be integrated into building envelopes to increase their thermal mass. An air-based BIPV/T-PCM system on the roof was designed to enhance ceiling ventilation by Lin et al. [115], where two PCM layers were integrated between the PV/T module and the ceiling to form an air channel as shown in Fig.

22a. The PCM layers played dual roles of serving as a part of ceiling insulation and provisionally storing the heat collected from the PV/T module for space heating when needed. While the ambient air fluctuated among 7.5–17.5 °C in winter, the outlet air through the channel was stably maintained among 20.6–24.5 °C for 24 hours with the aid of the heat collected by the module and subsequently stored by the PCM layers. The resulting warm air was quite suitable for indoor ventilation or space heating, offering decent thermal comfortableness for passive buildings in winter. They also designed a similar BIPV/T on the roof with PCM layers inside the envelopes (see Fig. 22b) [116]. Case studies indicated that the integration of the PCM layers remarkably increased the coefficient of thermal performance enhancement (CTPE) from 38.1% to 53.1%. They further adopted Taguchi-Fibonacci search method for optimizing the parameters including PCM type and thickness, air flow rate and wall insulation to maximize the CTPE, which was up to 72.22% [117].

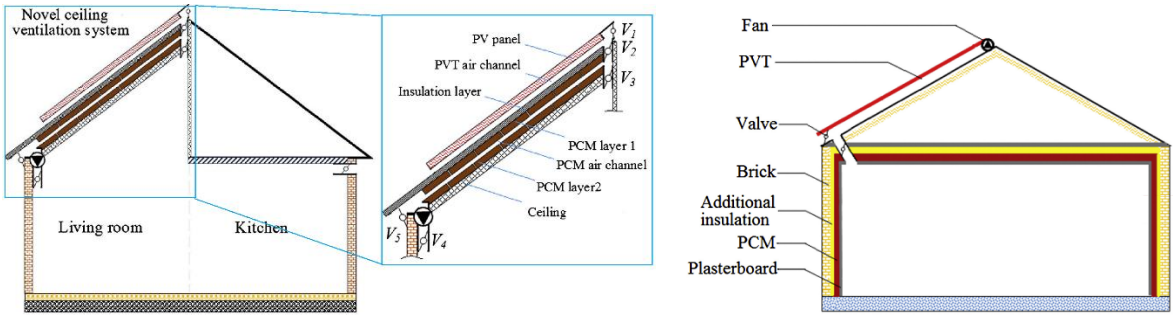

Fig. 22 Illustration of BIPV/T system installed on a house roof for enhanced ceiling ventilation and space heating: (a) integrating two PCM layers into the ceiling to form an air channel [115] and (b) integrating PCM layers into the envelopes [116, 117]

The above water-based and air-based BIPV/T-PCM systems were combined to form a new BIPV/T-PCM system on the roof as shown in Fig. 23 to enhance ceiling ventilation. Zhou et al. [118] focused on the PV performance of such a system rather than thermal performance. Liu et al. [119] claimed that the PCMs captured and stored the cooling energy in off-peak time and then used it in peak time for room or cell cooling. The PCM thickness, cooling water flow rate, inlet temperature and pipe diameter were optimized to maximize the equivalent overall

output energy. However, the stored free cooling energy in the night was not considered and the power consumption used to obtain 15 °C cooling water in summer was not allowed for since the inlet cooling water temperature was prescribed as 15 °C in optimized cases.

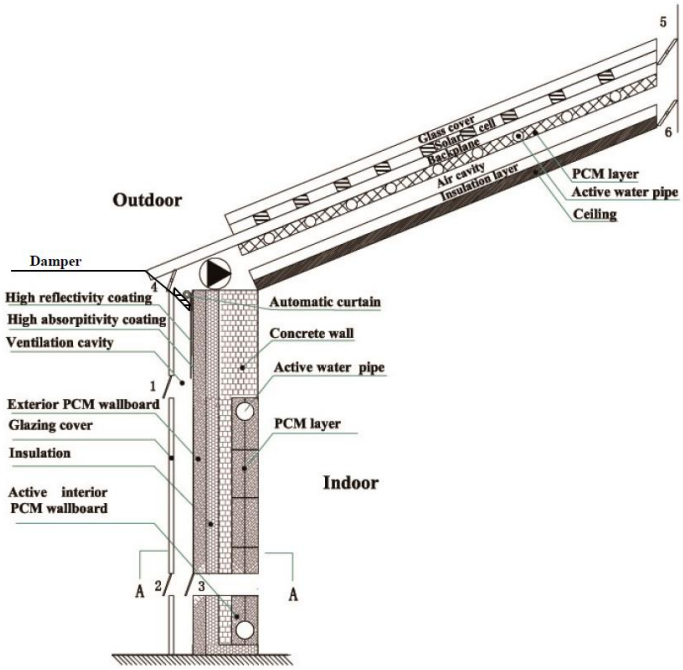

Fig. 23 Detailed construction of a water-based PV/T-PCM module installed on a house roof for enhanced ceiling ventilation integrated with a PCM-ventilated Trombe wall [119]

6.2 BIPV/T on the façade

A BIPV/T-PCM system on the façade was designed by Aelenei et al. [120], where an air channel/duct was constructed between a PV panel and a PCM board for ventilation (see Fig. 24a). In winter, the room air was extracted from a lower vent, flowed into the air channel to absorb heat, and then returned into the room for indoor heating. The building energy demands were therefore reduced. The thermal efficiency of such a system in winter was introduced as follows:

$$\eta_{th} = \frac{Q_{wall}+Q_{vent}}{Q_s \times A_{AP}}, \qquad (2)$$

where Q_{wall} and Q_{vent} are the heat flux into the room via the wall and transported by air ventilation, respectively. The air ventilation and latent heat absorption of PCM were also

helpful for reducing the PV temperature and thus improving the electrical efficiency. Pereira et al. [121] further extended the operation mode of the system in summer, where the external air ventilation was applied to limit the cell temperature rise and the heat penetration into the room. The thermal efficiency of such a system in summer was

$$\eta_{th} = \frac{Q_{vent} - Q_{wall}}{Q_s \times A_{AP}}. \qquad (3)$$

After optimizing the base cases from the air channel width, ventilation velocity, PCM thickness and latent heat, the overall energy efficiency increased from 24% to 64% for winter and from 4% to 32% for summer. The optimized PCM latent heat in summer was 1.9 times higher than that in winter. However, the role of PCM in the system was not explored in detail and the mechanical ventilation power consumption was not involved in the calculation.

Another similar BIPV/T-PCM system on the façade was proposed by Xiang et al. [62], where the PCM layer was located between the air duct and PV panel (see in Fig. 24b). In such a system, the PV temperature maintained below 48 °C via the PCM melting for about 9.7 h which sufficiently prevent PV overheating in the daytime, whereas it took almost 16.67 h to fully solidify the PCM under night natural ventilation which was notably reduced by the addition of internal fins. Fig. 25 demonstrated that the heat stored in PCM facilitated the formation of nature ventilation with heating the air. Consequently, the PCM layer is beneficial for suppressing the PV temperature rise and enhancing night ventilation to improve the electrical efficiency and indoor thermal comfort with reduced extra energy consumption for specific periods.

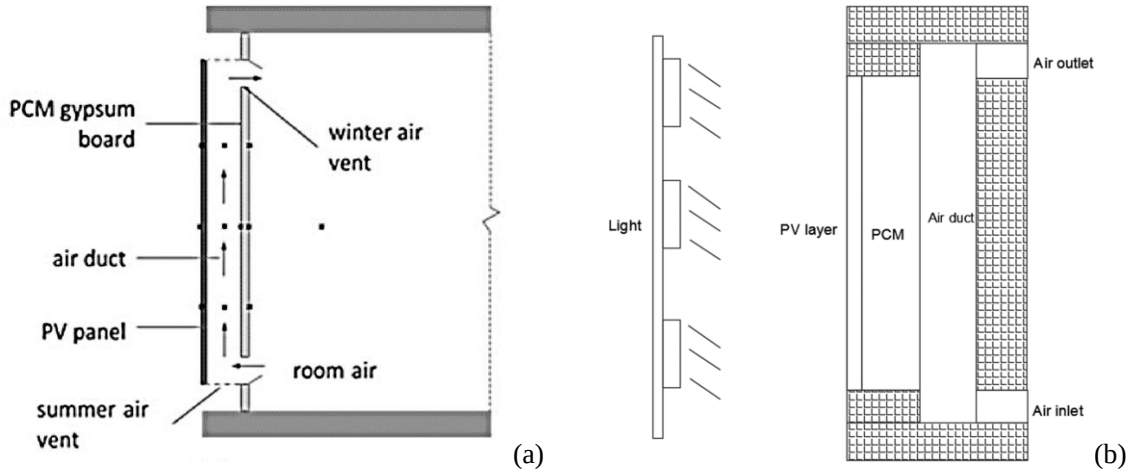

Fig. 24 System configuration of a BIPV/T-PCM system: (a) air duct is between PV panel and PCM [120, 121] and (b) PCM is between PV panel and air duct [62]

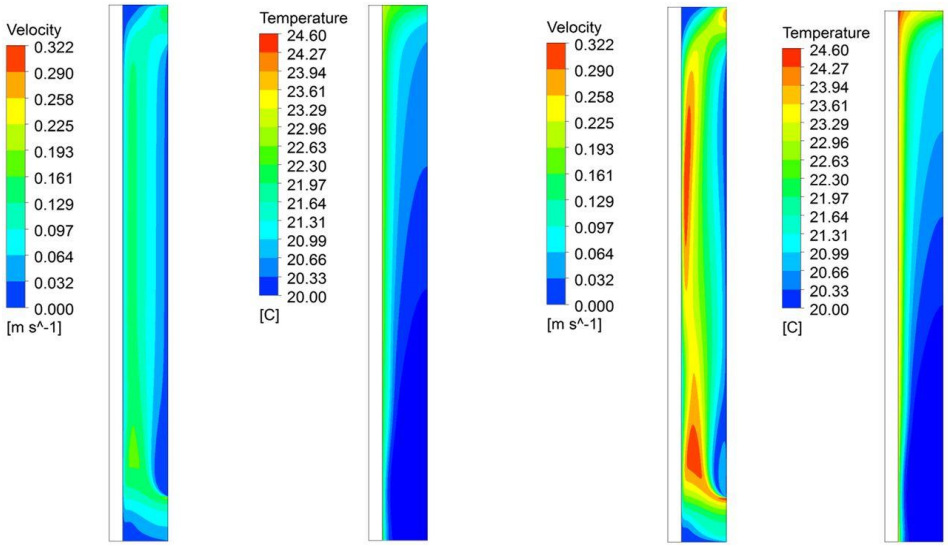

Fig. 25 Velocity and temperature fields in an air duct at 3000 s (left) and 10000 s (right) [62]

Similarly, the indoor ventilation in Fig. 24b should be changed to the exterior ventilation in summer, where the heated air is circulated outside as illustrated in Fig. 26. Čurpek et al. [122] reported that the integration of PCM in the summer mode significantly reduced the maximum PV temperature by 11–14 °C under the outside air temperature of 13–25 °C (see Fig. 27). As the outside temperature rose to 16–33 °C, the PCM of 27 °C melting point cannot be completely solidified with residual absorbed latent heat before the following diurnal cycle initiated, and therefore the maximum PV temperature was only decreased by 6–9 °C after integrating PCM. The thermal inertia of PCM notably enhanced the effects of the BIPV/T

ventilated façade serving as a thermal buffer in the daytime and as a warm coat in the night. They also believed that the investment costs of BIPV/T-PCM systems might hinder their economic viability. Kant, et al. [32] also deduced optimum designs for such a system in Fig. 26 with three types of PCMs (i.e. RT-25, n-octadecane and capric acid), where the obtained overall energy was maximized with an acceptable maximum PV temperature (<60 °C). The optimized parameters comprised PCM thickness, PV panel size, air flow rate and air gap width.

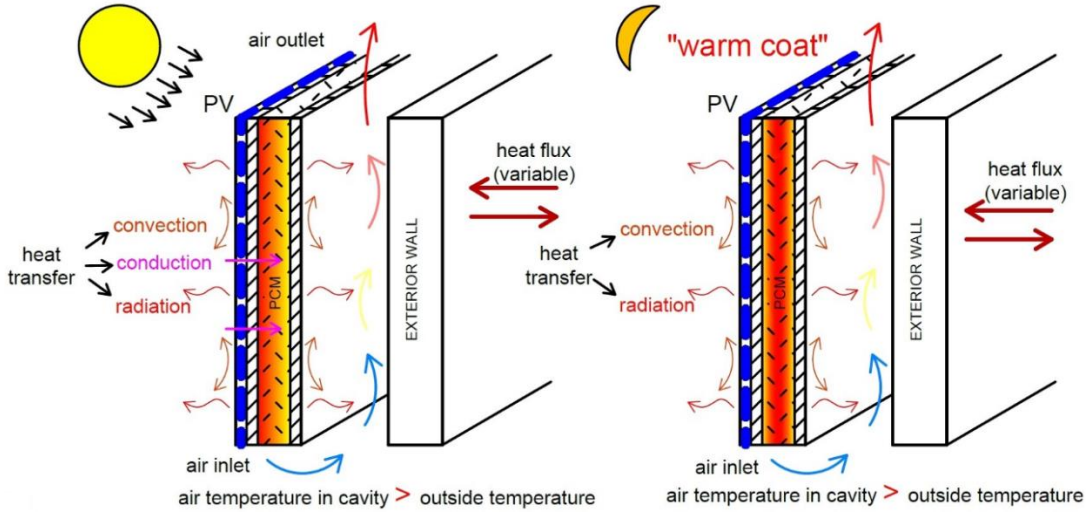

Fig. 26 Configuration and heat transfer modes of a BIPV/T-PCM ventilated façade in summer [122]

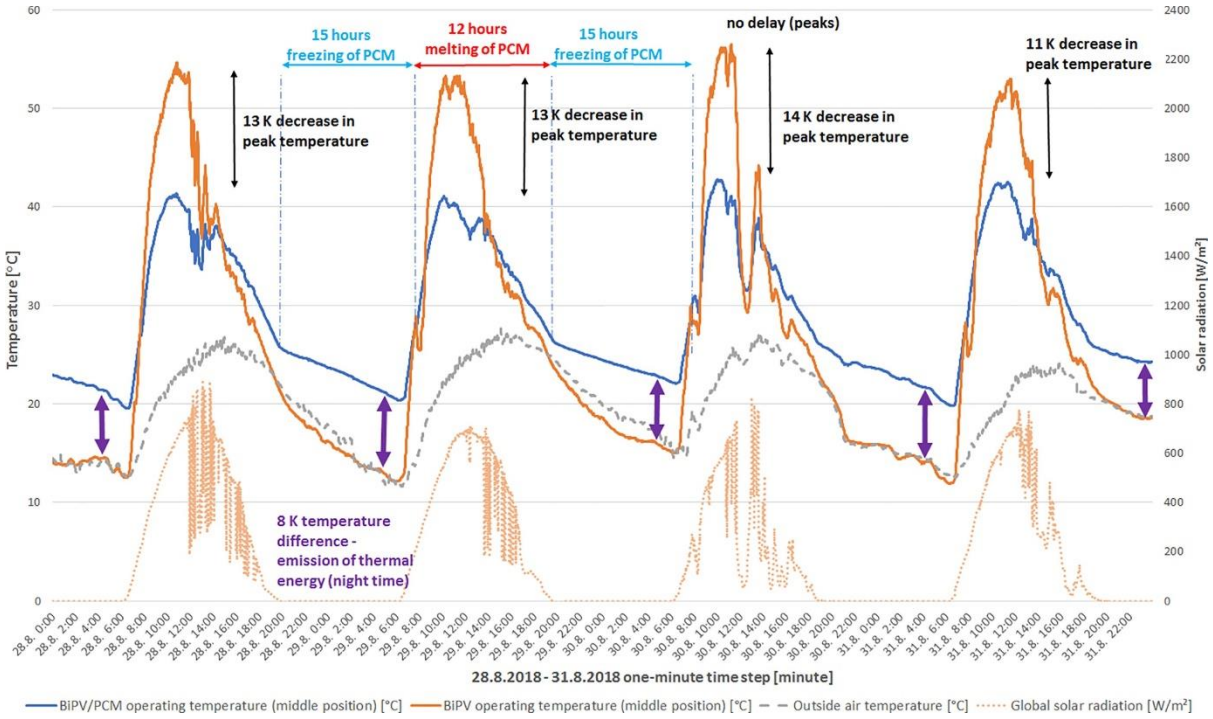

Fig. 27 Comparison of operating temperature between BIPV/T with and without PCM in summer [122]

A PCM layer was also integrated into a ventilated double-skin PV façade as shown in Fig. 28 to form a new BIPV/T-PCM system by Elarga et al. [45]. After integrating the PCM layer, the PV temperature dropped by over 20 °C and the monthly cooling load was also effectively lessened by 20%-30%. The combination of an appropriate melting temperature and a suitable ventilation scheme was a prerequisite to achieving the above benefits provided by the integration system. The selection of the melting temperature should make the PCM effectively melted during the daytime while the ventilation should effectively cool the melted PCM and make it return to its solid state during the night. Its role in improving indoor thermal comfort was not assessed in their study despite foreseeing a positive effect.

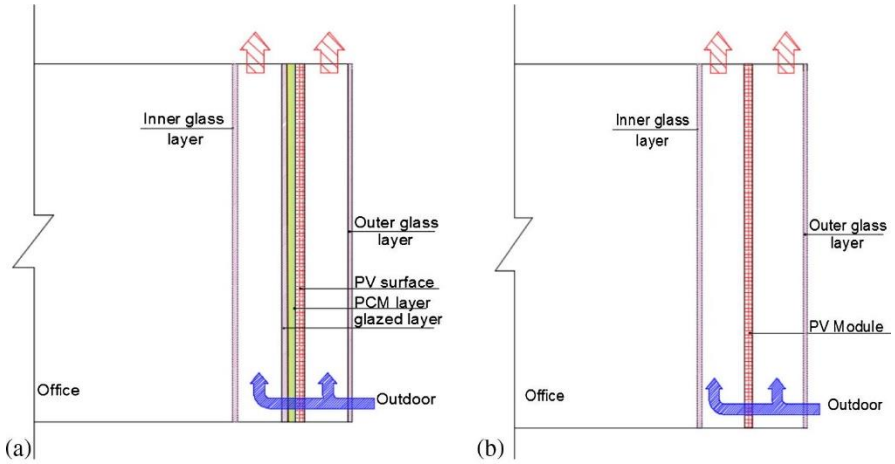

Fig. 28 BIPV/T of double-skin façades: (a) with a PCM layer; (b) without a PCM layer [45]

7. PV/T-PCM integrated with other energy conversion technologies

7.1 Heat pipe

Based on liquid-gas phase change heat transfer, a heat pipe (HPi) enables rapid transfer of a large amount of heat from its evaporation section to its condensation section [123]. Much work has been devoted to the integration of a PV/T module with various types of HPi, such as wire-meshed HPi [124], wickless gravity-assisted HPi [125], micro-channel HPi [126], loop HPi [127]. Only several studies have been performed on a combination of a PV/T module, PCM and HPi. Sweidan et al. [128] designed an HPi-PV/T-PCM hybrid system consisting of

an HPi, a PV panel and a PCM-water tank, to meet the requirements of an office building in hot water and electricity. The HPi evaporation section was placed on the rear surface of the PV panel to absorb heat while the condensation section was immersed in the tank to release heat. The payback period of the system proved to be 13.7 years. Diallo et al. [129] employed a loop HPi and a PCM-water-refringent triple heat exchanger instead of the PCM-water tank to reform the system (see Fig. 29), obtaining a 28% higher overall efficiency than a conventional one. Wang et al. [130] proposed a different HPi-PV/T-PCM system, where the PCM was located between the PV panel and the HPi. Such a system proved to be superior to the case without PCM [131] with an increment of 5-30% in the overall efficiency and an increment of 1.8-10.5 °C in the output water temperature. Kılkış [132] adopted a thermally pulsing HPi whose evaporation section was embedded in a PCM layer attached on the rear of a PV panel to control the PCM temperature and output heat via its condensation section.

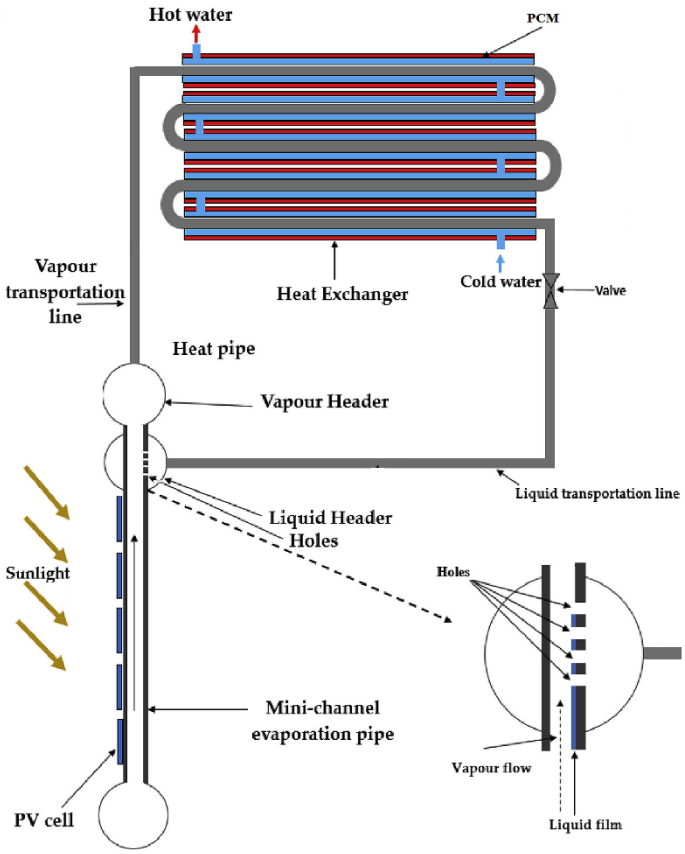

Fig. 29 Schematic of a loop HPi-PV/T-PCM system [129]

7.2 Thermoelectric device

A thermoelectric (TE) device can generate electricity by utilizing temperature difference, which is easily integrated with a PV panel to convert exhaust heat into electricity [133]. Various methods have been explored to further improve the performance of PV-TE hybrid systems, which include employing a two-stage TE device [134], segmented TE legs [135], heat pipe array [136], thermal interface materials [137] and so on. Adopting PCM is also a potential option. A concentrating PV-PCM-TE hybrid system as illustrated in Fig. 30a was established by Cui et al. [27]. They revealed that the integration of PCM with a suitable melting point alleviated the cell temperature fluctuations caused by time-varying solar irradiation and made the system operate at an optimal temperature, resulting in a relatively stable and higher efficiency. The heat stored in PCM at large irradiation was released to the TE device to generate electricity under weak or none irradiation, leading to an extreme rise in the overall efficiency nearby the sunset. For GaAs PV cells, the melting point of the selected PCM was 57 °C. Their experiment study further indicated the promising potential of the system to achieve the full-spectrum usage of solar energy [138]. Kılkış [132] proposed a different PV–PCM–TE hybrid system, where the cold end of the TE device was attached to the PCM layer to release heat and the hot end was connected with the backside of the PV panel via heat-conducting sheets to absorb heat. Motiei et al. [139] designed a PV-TE-PCM system where the PCM was attached at the cold side of TE (see Fig. 30b), which proved to experience better performance than the system without PCM. The PCM melting point and thickness need to be carefully chosen according to the ambient conditions to further increase the efficiency.

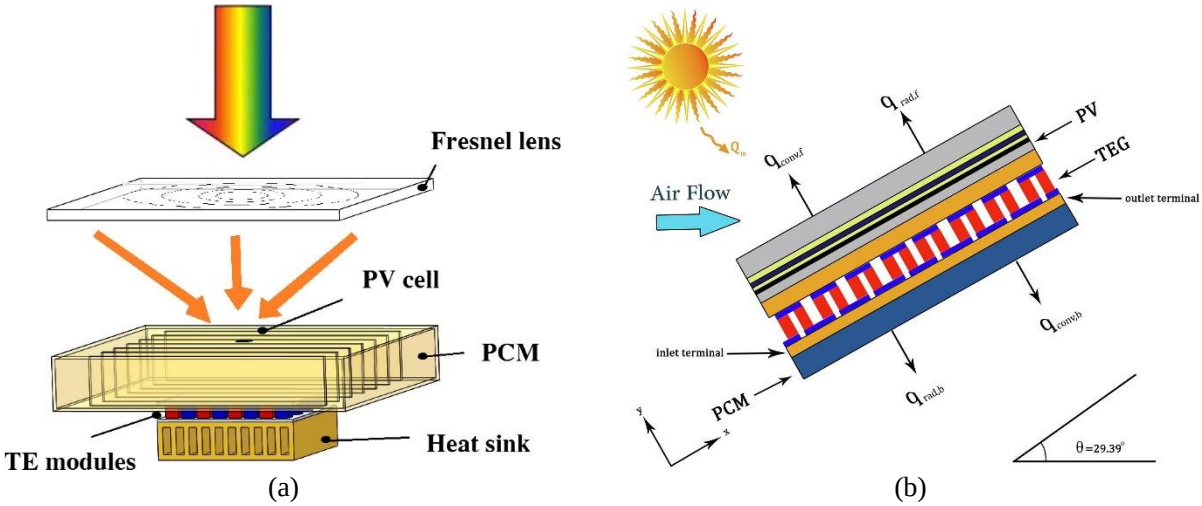

Fig. 30 Schematic of (a) PV-PCM-TE system [27] and (b) PV-TE-PCM system [139]

7.3 Heat pump

The heat collected in a PV/T module can serve as the heat source of the evaporator of a heat pump (HP) [140]. Much attention has been directed toward the integration of PV/T with an HP for space heating [141, 142], water heating [143], drying [144], etc. In a few studies, PCMs were introduced into PV/T-HP systems to increase the duration and stability of space heating. A coupled PV/T-HP-PCM system was established by Bigaila et al. [145], where the air heated in the PV/T module flowed through the evaporator to release heat and the heat produced in the condenser was stored in a PCM radiant panel for space heating. Yao et al. [67] designed a different PV/T-HP-PCM hybrid system as illustrated in Fig. 31, where the refrigerant directly evaporated in the PV/T module to absorb heat during a sunny day, the PCM was used to store the condensation heat of the HP and the generated electricity was used to drive the compressor. Simulations showed that such a hybrid system had a competitive COP of up to 5.79 while the electrical efficiency reached 17.77% and the thermal one was 55.76%. The resulting thermal energy grade was also elevated. Compared to a conventional HP system, the initial cost and maintenance cost of the proposed hybrid system was much higher due to the PV/T panels and underfloor heating equipment, while its operating cost was quite lower (i.e. lower than zero) as the spare electricity could be sold to power grid. Therefore, the total

cost of the proposed system would be lower than a conventional HP system after around four years of operation. But the detailed cost calculation method was unrevealed.

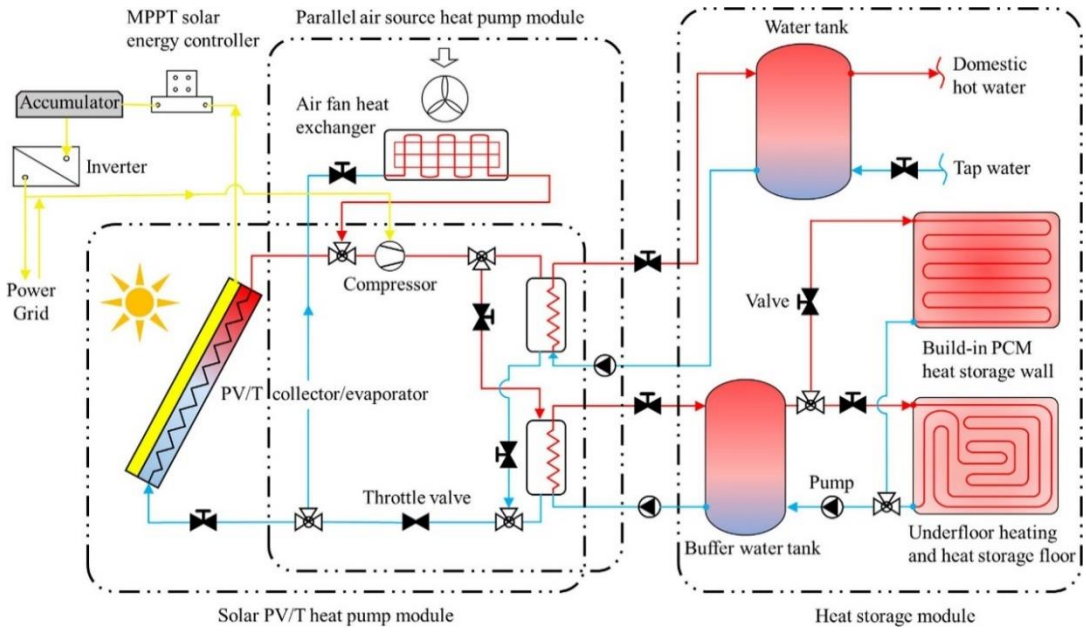

Fig. 31 Schematic of PV/T-HP-PCM system [67]

7.4 Ejector refrigeration cycle

An ejector is a heat-driven pressurizer that can replace a compressor in refrigeration cycles [146]. A solar thermal collector is generally integrated into an ejector refrigeration cycle to provide heat for producing high-temperature high-pressure vapor to drive the ejector [147], whereas integrating a PV/T module with an ejector refrigeration cycle is quite scarce. Ghorbani et al. [148] established a combined cooling, heating and power system via integrating PV/T modules, an ejector refrigeration cycle and a low-temperature PCM storage unit. The PV/T modules provided heat for the ejector to drive the refrigeration cycle while the PCM unit was applied to store cold for use at night. To obtain high electrical efficiencies, the working fluid temperature at the PV/T module outlet was not high enough to drive the ejector and therefore an auxiliary heater was adopted. They claimed that such a hybrid system had a thermal efficiency of 60.51% and an exergy efficiency of 50.84% as well as a payback period of 3.405 years. It's worth mentioning that a coupled solar system can be applied instead of the auxiliary heater to overcome the defect of low output temperature of PV/T, where a PV/T module and a

solar thermal collector are connected in series as Fig. 32 shows. Ma et al. [149] demonstrated a primary energy-saving efficiency of 83.48% for such a coupled system.

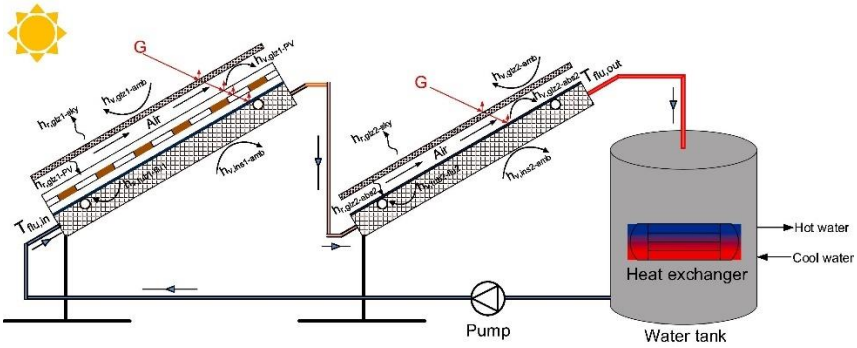

Fig. 32 Schematic of series connection of a PV/T and a solar thermal collector [149]

7.5 Solar still for fresh water production

The production efficiency of fresh water in a solar still which captures solar radiation via glass covers is far from being satisfactory. External solar thermal collectors [150], PCMs [151] or PV/T modules [152] have been adopted to improve the performance of a solar still. Hedayati-Mehdiabadi et al. [153] simultaneously equipped a PV/T module and a PCM layer into a basin-type solar still as Fig. 33 presents. In the system, the PV/T module preheated saline water before flowing into the basin to elevate desalination efficiency in the basin while it supplied the electricity to transport saline water during the daytime. The PCM enabled fresh water production in the night because it stored the heat loss of the basin in the daytime and hence heat was available in the night. Such an integration system potentially achieved continuous fresh water production during the whole day.

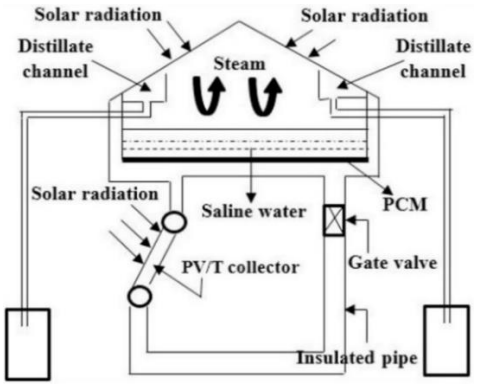

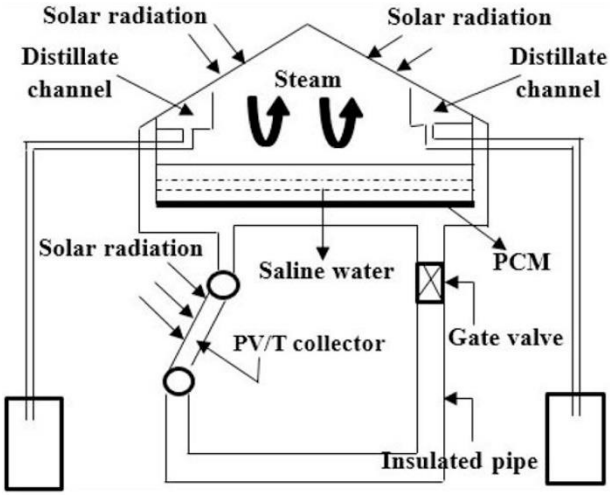

Fig. 33 Basin-type solar still integrated with PV/T and PCM [153]

7.6 Proton Exchange Membrane electrolyzer for hydrogen production

Hydrogen as a clean fuel is a promising alternative to fossil fuels [154]. Hydrogen can be generated from water via electrolyzers powered by PV cells, while the heat from the PV cells can be used to elevate the electrolysis reaction kinetics [155]. Therefore, several studies have been performed on the integration of PV/T modules with electrolyzers [156, 157]. Babayan et al. [34] further integrated a PV/T-PCM module with a proton exchange membrane (PEM) electrolyzer to produce hydrogen (see Fig. 34). The electricity produced via the PV/T module was applied to actuate the water decomposition reaction while the hot water produced by the PV/T module was injected into the electrolyzer as the reactant. The PCM was used to further cool the PV cell and extend the supply time of hot water. They revealed that the proposed system achieved 5.32% higher hydrogen production than the case without PCM.

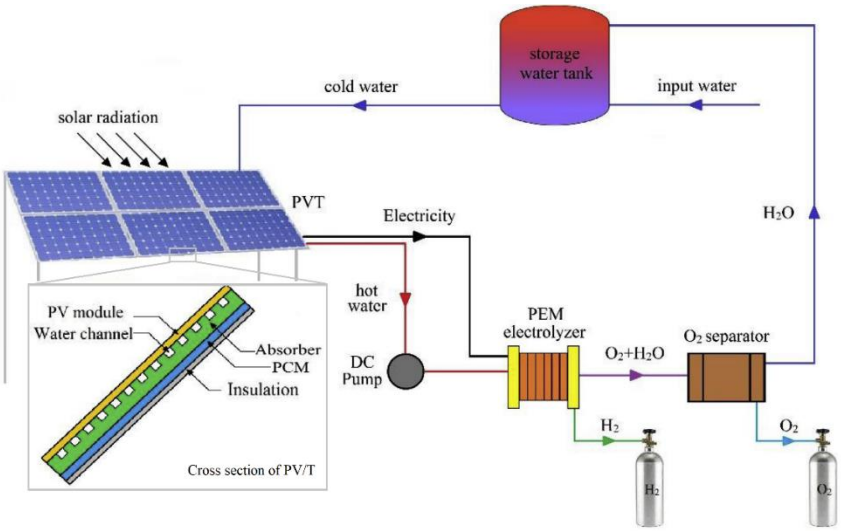

Fig. 34 Schematic of PEM electrolyzer integrated with the PV/T-PCM module [34]

8. Conclusions and Outlook

8.1 Summary of conclusions

This paper reviews the recent research progress on the utilization of PCMs in standalone PV/T modules, BIPV/T systems and PV/T systems integrated with other energy conversion technologies. PCMs can be integrated in the form of bulk or MPCM slurry. The performance evaluation indexes of PV/T systems mainly include power output, energy and exergy efficiencies under the thermal, electrical and overall terms. PCMs adopted in PV/T systems available include various types of paraffins, acids and their eutectic mixtures, hydrated salts and eutectic salts. Various types of paraffins are the most prevalent. The melting temperatures of PCMs applied in flat-plate PV/T are within the range of 14–57 ºC, while those in concentrated PV/T are within the range of 47–147 ºC.

Bulk PCMs have been integrated into standalone PV/T modules with different configurations regarding the relative position between the working fluid channel and the PCM layer. In most cases, the PCM layer is attached to the rear of the absorber plate to absorb and store heat through melting. Integrating PCM generally has four purposes: (1) PV panel cooling; (2) anti-freezing; (3) thermal efficiency improvement; and (4) heat supply regulation, e.g.

increasing the duration and flexibility. After integrating PCM, the cell temperature is effectively decreased and thus the electrical efficiency is enhanced. Both the thermal and overall efficiencies are elevated only when the heat stored in PCM is extracted for thermal applications. The PCM melting point is the most critical parameter for a PV/T-PCM module. Only a suitable melting point can ensure the effective module operation and the optimum melting point depends on the local climate conditions. The operation scheme based on the adjustment of the flow rate should be precisely tailored according to the varying ambient temperature and solar irradiation to ensure the optimal solidification/melting period of PCM and achieve the desired performance.

Under a suitable MPCM concentration and melting point, the PV/T module with the MPCM slurry performs better than that with water in all types of efficiencies. A higher MPCM concentration is conducive to improving module performance as long as the turbulent flow state is maintained, whereas the performance is remarkably impaired as the flow turns into the laminar state. Both the thermal and electrical efficiencies are improved by selecting a lower melting point within a certain range, while the overall exergy efficiency is elevated by adopting a higher melting point.

PCMs are integrated into BIPV/T systems in the form of an independent storage device, being embedded in a roof, interior or external wall, or being attached to the rear of the PV panels. The fluctuated climatic conditions remarkably influence energy flows between outdoor and indoor spaces, which should be accurately tailored to meet the indoor thermal comfort with minimizing the required energy. The integration of PCM brings the flexibility of adjustment in energy flows under wavy solar radiation and ambient temperature. Besides cooling the PV panel and storing heat for later use, the integrated PCMs play a role in facilitating air ventilation for indoor thermal comfort improvement or preventing exterior heat penetration for cold load reduction, which cut down the building energy consumption.

The integration of PV/T-PCM with other energy conversion technologies further improves the overall performance of various integration systems and accomplishes a variety of applications, such as temperature-difference power generation, thermal energy grade promotion, refrigeration, as well as water and hydrogen production.

This review can facilitate further improvements in such an emerging solution for renewable energy utilization. To better understand the state of the art in the PV/T-PCM technology, the performance data on PV/T-PCM systems available in the literature are summarized in Table 5.

Table 5 Performances of PV/T-PCM modules/systems available in the literature.

References	Country	Working medium	PCM Melting temperature (°C)	PV cell temperature (°C)	Electrical efficiency (%)	Thermal efficiency (%)	Overall efficiency (%)	Exergy efficiency (%)	Solar irradiation (W/m^2)	Ambient temperature (°C)	Approach
Standalone PV/T with bulk PCMs											
Imam et al. [60]	Bangladesh	Water + PCM	56	20–85	N.A.	42–50	55–63[a]	N.A.	1050[^] (Con.)	N.A.	Exp.
Kazemian et al. [52]	China	Water + PCM	46–48	48.2[*]	13.40[*]	74.17[*]	87.57[*, a]	13.75[*, a]	450–900	27–33	Exp.
		Water/50% EG + PCM	46–48	52.9[*]	13.11[*]	72.28[*]	85.39[*, a]	13.65[*, a]			
		EG + PCM	46–48	54.9[*]	12.91[*]	69.03[*]	81.94[*, a]	13.56[*, a]			
Kazemian et al. [69]	China	Water	–	65.2	12	43.9	N.A.	N.A.	800	30	Num.
		Water + PCM	55	55.6	13	57.3	N.A.	N.A.			
Kazemian et al. [75]	China	Water + PCM	40	10[^]	16.21[*]	27.80[*]	44.81[*, a]	17.16[*, a]	600[^]	0–6	Num.
				44[^]	14.22[*]	58.67[*]	73.65[*, a]	15.41[*, a]	880[^]	15–31	
				50[^]	13.87[*]	72.88[*]	86.75[*, a]	15.18[*, a]	1030[^]	27–34	
Modjinou et al. [29]	China	Water	–	72.5[^]	7.88[*]	23.90[*]	31.78[*, a]	N.A.	200–1000	18.5–27	Exp.
		Water + HPi	–	75[^]	7.78[*]	27.75[*]	35.53[*, a]	N.A.			
		Water + PCM	15	62.5[^]	7.95[*]	28.76[*]	36.71[*, a]	N.A.			
Su et al. [68]	China	Air	–	31–77.4	9.2–11.6	19	35–39[&, a]	N.A.	1000[^]	28.5–37.4	Num.
		Air + PCM	28	27.2–70	9.6–11.9	13.5–43.5	33–64[&, a]	N.A.			
Wang et al. [130]	China	Water + PCM + HPi	52.1	28–65	7.6[*]	51.3[*]	58.9[*, a]	N.A.	300	25–28	Exp.
				28–85	5.8[*]	27.0[*]	32.8[*, a]	N.A.	900	25–28	
Xu et al. [41]	China	Water + PCM	37	38–53	12.1[*]	78.7[*]	90.8[*, a]	N.A.	250–1000	25–28	Exp.
Yang et al. [37]	China	Water	–	66.6[^]	6.98	58.38	63.93[b]	N.A.	800	28	Exp.
		Water + PCM	30.1	56.7[^]	8.16	70.34	76.87[b]	N.A.			
Yang et al. [38]	China	Water + PCM	30.1	57.0	8.2	71.8	78.36[b]	33.4[a]	800	28	Num.
Yao et al. [67]	China	HP (R134A) + Water + PCM	37	N.A.	17.77	55.76	75.49[$]	N.A.	600	15	Num.
Yuan et al. [73]	China	Water	–	29–45.3	11.9[*]	44.5[*]	N.A.	N.A.	200–850	9.2–13.5	Exp.
		Water + PCM	15	21–38.8	12.1[*]	42.3[*]	N.A.	N.A.			
Salem et al. [64]	Egypt	Water + PCM	31	39.5[*]	10.8*	40[*]	N.A.	11.2[*, b]	632.5–650.8	35.4–37.2	Exp.
		Water + 1 wt% Nano-Al_2O_3/PCM	31	35.5[*]	11.5*	34[*]	N.A.	11.8[*, b]			
Gaur et al. [42]	France	Water	–	15–51.4	16.5[*]	52.34[*]	N.A.	N.A.	800[^]	1–12	Num.
		Water + PCM	37	15–46.8	16.87[*]	84.01[*]	N.A.	N.A.			
		Water	–	20–69.2	15.4[*]	43.73[*]	N.A.	N.A.	900[^]	15–24	
		Water + PCM	37	20–53.9	16.3[*]	59.66[*]	N.A.	N.A.			
AL-Musawi et al. [72]	Hungary	Water + PCM	31	35.7	14.35	32	N.A.	N.A.	1000	35	Num.
		3 wt% Nano-SiO_2/Water + PCM	31	35.6	14.38	40	N.A.	N.A.			

Preet et al. [35]	India	Water	–	30.5-58	11.55*	62.37*	N.A.	N.A.	1150^	N.A.	Exp.
		Water + PCM	28	30.5-55	13.0*	35.4*	N.A.	N.A.			
Babayan et al. [34]	Iran	Water	–	70.2^	13.1*	N.A.	32.50*, a	13.25*, a	1022^	21.2–36.1	Num.
		Water + PCM	35	59.2^	14.3*	N.A.	35.04*, a	13.92*, a			
			44	62.4^	14.0*	N.A.	32.86*, a	13.78*, a			
			50	64.5^	13.8*	N.A.	32.67*, a	13.67*, a			
Hosseinzadeh et al. [51]	Iran	0.2 wt% Nano-ZnO/Water	–	51^	13.44*	39.86*	53.30*, a	12.37*, a	600–1000	25–31	Exp.
		0.2 wt% Nano-ZnO/Water + PCM	46–48	45^	14.05*	51.66*	65.71*, a	13.61*, a			
Kazemian et al. [50]	Iran	Water + PCM	46–48	41.3^	14.03*	70.46*	84.49*, a	14.37*, a	440–850	N.A.	Exp.
		Water/50% EG + PCM	46–48	42.5^	13.89*	63.72*	77.61*, a	14.42*, a			
		EG + PCM	46–48	47.6^	13.69*	52.95*	66.64*, a	15.13*, a			
Mousavi et al. [28]	Iran	Water	–	71	12.2	86	N.A.	15.52a	600	25	Num.
		Water + PCM	29	55	13.1	81	N.A.	15.6a			
		Water + PCM/MF	29	33	14.5	69	N.A.	16.7a			
Salari et al. [82]	Iran	Water + PCM	40	42.3	13.83	41.41	55.24a	N.A.	1000	30	Num.
		6 wt% Nano-MgO/Water + PCM	40	41.3	13.89	46.18	60.07a	N.A.			
		6 wt% MWCNT/Water + PCM	40	41.3	13.91	47.17	61.08a	N.A.			
Sardarabadi et al. [49]	Iran	Water	–	52^	N.A.	N.A.	N.A.	12.23*, a	600–1000	25.5–30.5	Exp.
		Water + PCM	46–48	45^	N.A.	N.A.	N.A.	13.17*, a			
		0.2wt% Nano-ZnO/Water + PCM	46–48	45^	N.A.	N.A.	N.A.	13.42*, a			
Sweidan et al. [128]	Lebanon	Water + PCM	33	N.A.	10.56^	19.08^	46.87&, ^, a	N.A.	N.A.	N.A.	Exp.
Al-Waeli et al. [44, 53]	Malaysia	Water	–	45.2^	9.92^	35.4^	N.A.	N.A.	200–720	24–37	Exp.
		Water + PCM	49	42.2^	12.32^	50.5^	N.A.	N.A.			
		3wt% Nano-SiC/Water + 0.1wt% Nano-SiC/PCM	49	39.5^	13.70^	72^	N.A.	N.A.			
Fayaz et al. [47]	Malaysia	Water	–	74.6	12.28	77.5	89.78a	N.A.	1000	27	Exp.
		Water + PCM	44.8	69.1	12.59	70.8	83.39a	N.A.			
Hossain et al. [40]	Malaysia	Water + PCM	44–46	52–68	10.29*	73.7*	N.A.	12.19*, a	300–1000	30–36	Exp.
Sopian et al. [54]	Malaysia	Nano-SiC/Water + Nano-SiC/PCM	49	45*	13.7*	72*	85.7*, a	N.A.	150–720	31*	Exp.
Abdelrazik et al. [80]	KSA	Nano-GR/Water	–	52.5	10.5	67.23	77.73a	N.A.	921	25	Num.
		Nano-GR/Water + PCM	N.A.	66.5	9.75	61.21	70.96a	N.A.			
		Nano-GR/Water +PCM+ Nano-Ag/Water (OF)	N.A.	38.9	11.24	79.01	90.25a	N.A.			
Lari et al. [36]	KSA	Nano-Ag/Water + PCM	28	26–34	12.6*	55.5*	N.A.	N.A.	N.A.	N.A.	Exp.
Maatallah et al. [55]	KSA	Water + PCM	57	60^	13.7*	26.9*	40.6*, a	N.A.	250–800	32–36	Exp.
Simón-Allué et al. [87]	Spain	Water	–	N.A.	15*	N.A.	55&, *, b	N.A.	800–1000	25–38	Exp.
		Water + PCM	44–46	N.A.	14.9*	N.A.	56&, *, b	N.A.			

Ceylan et al. [71]	Turkey	Air +PCM	47	15–41	10.6–12.1	N.A.	10-82[&, a]	N.A.	2200[^] (Con.)	21–41	Exp.
Ergün et al. [57]	Turkey	Water + PCM	47	58[^]	N.A.	N.A.	N.A.	9.2[*, a]	400–1150	N.A.	Exp.
		Water + 5 wt% Nano-Al_2O_3/PCM	47	56[^]	N.A.	N.A.	N.A.	10[*, a]			
Diallo et al. [129]	UK	Water + HPi	–	N.A.	11	38	49[a]	N.A.	800	25	Num.
		Water + PCM + HPi	44	41.1	12.2	55.6	67.8[a]	N.A.			
Tabet Aoul et al. [59]	UAE	Water	–	110[^]	16.5–22	14[^]	18–35[#]	N.A.	2156[^] (Con.)	24–42	Exp.
		Water + PCM	56.9	86[^]	18–22	24[^]	20–40[#]	N.A.			
Standalone PV/T with MPCM slurry											
Chen et al. [108]	China	Water	–	28-58	13.2[*]	19.3[*]	49.6[&, *, b]	N.A.	156–850	23-37	Exp.
		30% PCM particles/Water	35	28-55	14.0[*]	24.3[*]	59.3[&, *, b]	N.A.			
Liu et al. [103]	China	Water + Air	–	28–34.2	8.74–8.97	68.6–70.2	77.3–78.8[#]	N.A.	168–890	17.1–22.6	Num.
		10 wt% MPCM/Water + Air	28	28–33	8.79–8.97	68.6–71.8	77.3–80.6[#]	9.8–11.4[#, b]			
Liu et al. [105]	China	Water	–	28.2–42.4	11.2–11.8	55.3–71.9	61.0–77.8[a]	N.A.	140–1010	27.2–31.6	Num.
		10 wt% MPCM/Water	28.4	28.1–37.7	11.4–11.8	58.6–78.5	64.3–84.4[a]	N.A.			
Eisapour et al. [107]	Iran	Water	–	40	11.19	62.47	N.A.	13.25[a]	1000	20	Num.
		15 wt% MPCM/Water	37	38.2	11.28	63.28	N.A.	13.13[a]			
		9% Nano-Ag/15 wt% MPCM/Water	37	37.4	11.33	67.14	N.A.	13.26[a]			
Qiu et al. [26]	UK	5 wt% MPCM/Water	28.4	40.5	15.7	44.6	59.9[#]	N.A.	1000	20	Num.
Qiu et al. [109]	UK	10 wt% MPCM/Water	28.4	31.9	14.1	68.8	81.5[#]	N.A.	600	29.5	Exp.
Yu et al. [106]	UK	Water	–	45	11.0	64.1	75.1[a]	12.0[a]	1000	20	Num.
		20 wt% MPCM/Water	37	42	11.2	67.0	78.2[a]	12.2[a]			
Building-integrated PV/T with bulk PCMs											
Fiorentini et al. [61]	Australia	Air + PCM	22	N.A.	8.2[*]	9[*]	17.2[*, a]	N.A.	200-800	N.A.	Exp.
Lin et al. [115]	Australia	Air + PCM	21–25	44.2[^]	8.31[*]	12.5[*]	N.A.	N.A.	530[^]	7–17	Exp.
				71.7[^]	8.26[*]	13.6[*]	N.A.	N.A.	1000^	20–28	
Aelenei et al. [120]	Portugal	Air + PCM	18-23	18–56	10[^]	10[^]	20[^, a]	N.A.	22-866	8.4–13	Num.
Pereira et al. [121]	Portugal	Air + PCM	18-23	45[^]	10[*]	54[*]	64[*, a]	N.A.	866[^]	4–12	Num.
				46[^]	5[*]	27[*]	32[*, a]	N.A.	900[^]	23–38	
Yin et al. [112]	USA	Water + PCM	N.A.	38	11.4	53.9	65.3[a]	N.A.	1100	25	Exp.

[a] or [b] denotes adopted calculation or definition expression as described in Table 2; [^] denotes daily maximum value; [*] denotes daily (or monthly) average value; [&] denotes primary-energy saving efficiency; [$] denotes overall energy efficiency considering condensation heat; [#] denotes net efficiency considering power pump consumption; N.A. denotes not available; Con. denotes concentrated; EG denotes ethylene glycol; HPi denotes heat pipe; MF denotes metal foam; HP denotes heat pump; Nano denotes nanoparticles; MWCNT denotes multiwalled carbon nanotube; GR denotes graphene; OF denotes optical filter; Exp. denotes experimental; Num. denotes numerical.

8.2 Outlook for PV/T-PCM technologies

Based on the comprehensive review in this paper, the following topics on PV/T-PCM are worth addressing in future research:

(1) PCMs with a suitable melting temperature, a large latent heat and a high thermal conductivity are in demand. It is necessary to develop new PCMs to modulate the melting temperature and latent heat or develop composite PCMs to improve the thermal conductivity. The phase segregation, thermal reliability, subcooling and leakage issues of PCMs remain largely unaddressed, especially under the varying solar irradiation and ambient temperature.

(2) Performance comparisons between various configurations of PV/T-PCM modules and the corresponding optimum design are scarcely addressed. Guidance on the design and configuration optimization of PVT-PCM modules should be provided. The grade of generated thermal energy needs to be elevated.

(3) Experimental testing is required to explore the stability of MPCM slurry in PV/T modules during the circulation operation, such as possible agglomeration, sedimentation, stratification and shell cracking of MPCM. A combination of MPCM particles with different melting points in one slurry could be adopted to tackle the varying solar irradiation.

(4) It is still requisite to develop more effective and compact designs of BIPV/T-PCM systems. More sophisticated daily operation strategies for the façade/ceiling ventilation are required to give rise to high-efficiency melting/solidification processes of PCM. Seasonal ventilation regime or thermal storage could be considered to improve the year-round system performances for achieving building energy efficiency or even net-zero energy building.

(5) The studies on the integration of PV/T-PCM with various energy conversion technologies remain limited. Modifications need to be performed on the existing integration systems for more efficient energy outputs. The integration could be extended to broader energy conversion technologies for realizing more functions.

(6) In various PV/T-PCM integrated systems, a PCM heat storage unit or heat exchanger is the key component. In view of the complexity caused by varying climate conditions, it is required to carry out in-depth research or propose innovative designs for a PCM heat storage unit or heat exchanger to meet the demand of integrated systems.

(7) The current numerical models for PV/T-PCM systems include 1D model based on the thermal network and 2D or 3D model based on CFD. The accuracy of 1D model is not ensured. The 2D or 3D model is quite time-consuming especially for predicting the yearly performances. Very precise models with a fast prediction (e.g. coupling the 1D and 3D models) should be developed for fast design optimization and performance prediction.

(8) The design and optimization of PV/T-PCM systems should be performed considering the annual variation of climate conditions for selecting PCM melting point and mass, module configuration and system integration. In view of the probable performance degradation of PCMs in the long term, the system life cycle test must be implemented to clarify their long-term performances for practical applications.

Acknowledgements

The authors would like to acknowledge the financial supports of the Innovation Technology Fund (ITS/171/16FX) and the Research Impact Fund (RC2H) of the Hong Kong SAR Government.

References

[1] Kumar A, Baredar P, Qureshi U. Historical and recent development of photovoltaic thermal (PVT) technologies. Renew Sust Energ Rev. 2015;42:1428-36.
[2] Joshi SS, Dhoble AS. Photovoltaic - Thermal systems (PVT): Technology review and future trends. Renew Sust Energ Rev. 2018;92:848-82.
[3] Sultan SM, Efzan MNE. Review on recent Photovoltaic/Thermal (PV/T) technology advances and applications. Sol Energy 2018;173:939-54.
[4] Brahim T, Jemni A. Economical assessment and applications of photovoltaic/thermal hybrid solar technology: A review. Sol Energy 2017;153:540-61.
[5] Rejeb O, Gaillard L, Giroux-Julien S, Ghenai C, Jemni A, Bettayeb M, et al. Novel solar PV/Thermal collector design for the enhancement of thermal and electrical performances. Renew Energy. 2020;146:610-27.
[6] Das D, Kalita P, Roy O. Flat plate hybrid photovoltaic- thermal (PV/T) system: A review on design and development. Renew Sust Energ Rev. 2018;84:111-30.
[7] Islam MM, Pandey AK, Hasanuzzaman M, Rahim NA. Recent progresses and achievements in photovoltaic-phase change material technology: A review with special treatment on photovoltaic thermal-phase change material systems. Energy Convers Manage 2016;126:177-204.
[8] Kuo CFJ, Yang PC, Umar ML, Lan WL. A bifacial photovoltaic thermal system design with parameter optimization and performance beneficial validation. Appl Energy 2019;247:335-49.
[9] Han X, Xue D, Zheng J, Alelyani SM, Chen X. Spectral characterization of spectrally selective liquid absorption filters and exploring their effects on concentrator solar cells. Renew Energy. 2019;131:938-45.
[10] Liang H, Wang F, Zhang D, Cheng Z, Zhang C, Lin B, et al. Experimental investigation of cost-effective ZnO nanofluid based spectral splitting CPV/T system. Energy. 2020;194:116913.
[11] Tomar V, Tiwari GN, Bhatti TS, Norton B. Thermal modeling and experimental evaluation of five different photovoltaic modules integrated on prototype test cells with and without water flow. Energy Convers Manage 2018;165:219-35.
[12] Al-Shohani WAM, Sabouri A, Al-Dadah R, Mahmoud S, Butt H. Experimental investigation of an optical water filter for Photovoltaic/Thermal conversion module. Energy Convers Manage 2016;111:431-42.
[13] Han X, Chen X, Sun Y, Qu J. Performance improvement of a PV/T system utilizing Ag/CoSO4-propylene glycol nanofluid optical filter. Energy. 2020;192:116611.
[14] Ramdani H, Ould-Lahoucine C. Study on the overall energy and exergy performances of a novel water-based hybrid photovoltaic-thermal solar collector. Energy Convers Manage 2020;222:113238.
[15] Abdelrazik AS, Saidur R, Al-Sulaiman FA. Investigation of the performance of a hybrid PV/thermal system using water/silver nanofluid-based optical filter. Energy. 2021;215:119172.
[16] Günther E, Hiebler S, Mehling H, Redlich R. Enthalpy of Phase Change Materials as a Function of Temperature: Required Accuracy and Suitable Measurement Methods. Int J Thermophys 2009;30:1257-69.
[17] Abokersh MH, Osman M, El-Baz O, El-Morsi M, Sharaf O. Review of the phase change material (PCM) usage for solar domestic water heating systems (SDWHS). Int J Energy Res 2018;42:329-57.
[18] Yazdanifard F, Ameri M. Exergetic advancement of photovoltaic/thermal systems (PV/T): A review. Renew Sust Energ Rev. 2018;97:529-53.
[19] Abbas N, Awan MB, Amer M, Ammar SM, Sajjad U, Ali HM, et al. Applications of nanofluids in photovoltaic thermal systems: A review of recent advances. Physica A 2019;536:26.
[20] George M, Pandey AK, Abd Rahim N, Tyagi VV, Shahabuddin S, Saidur R. Concentrated photovoltaic thermal systems: A component-by-component view on the developments in the design, heat transfer medium and applications. Energy Convers Manage 2019;186:15-41.
[21] Abdelrazik AS, Al-Sulaiman FA, Saidur R, Ben-Mansour R. A review on recent development for the design and packaging of hybrid photovoltaic/thermal (PV/T) solar systems. Renew Sust Energ Rev. 2018;95:110-29.
[22] Jia YT, Alva G, Fang GY. Development and applications of photovoltaic-thermal systems: A review. Renew Sust Energ Rev. 2019;102:249-65.

[23] Diwania S, Agrawal S, Siddiqui AS, Singh S. Photovoltaic-thermal (PV/T) technology: a comprehensive review on applications and its advancement. International Journal of Energy and Environmental Engineering. 2020:22.
[24] Riaz A, Liang RB, Zhou C, Zhang JL. A review on the application of photovoltaic thermal systems for building facades. Build Serv Eng Res Technol. 2020;41:86-107.
[25] Huang BJ, Lin TH, Hung WC, Sun FS. Performance evaluation of solar photovoltaic/thermal systems. Sol Energy 2001;70:443-8.
[26] Qiu Z, Zhao X, Li P, Zhang X, Ali S, Tan J. Theoretical investigation of the energy performance of a novel MPCM (Microencapsulated Phase Change Material) slurry based PV/T module. Energy. 2015;87:686-98.
[27] Cui T, Xuan Y, Li Q. Design of a novel concentrating photovoltaic–thermoelectric system incorporated with phase change materials. Energy Convers Manage 2016;112:49-60.
[28] Mousavi S, Kasaeian A, Shafii MB, Jahangir MH. Numerical investigation of the effects of a copper foam filled with phase change materials in a water-cooled photovoltaic/thermal system. Energy Convers Manage 2018;163:187-95.
[29] Modjinou M, Ji J, Yuan W, Zhou F, Holliday S, Waqas A, et al. Performance comparison of encapsulated PCM PV/T, microchannel heat pipe PV/T and conventional PV/T systems. Energy. 2019;166:1249-66.
[30] Browne MC, Norton B, McCormack SJ. Heat retention of a photovoltaic/thermal collector with PCM. Sol Energy 2016;133:533-48.
[31] Abdelrazik AS, Al-Sulaiman FA, Saidur R. Numerical investigation of the effects of the nano-enhanced phase change materials on the thermal and electrical performance of hybrid PV/thermal systems. Energy Convers Manage 2020;205:112449.
[32] Kant K, Pitchumani R, Shukla A, Sharma A. Analysis and design of air ventilated building integrated photovoltaic (BIPV) system incorporating phase change materials. Energy Convers Manage 2019;196:149-64.
[33] Malvi CS, Dixon-Hardy DW, Crook R. Energy balance model of combined photovoltaic solar-thermal system incorporating phase change material. Sol Energy 2011;85:1440-6.
[34] Babayan M, Mazraeh AE, Yari M, Niazi NA, Saha SC. Hydrogen production with a photovoltaic thermal system enhanced by phase change materials, Shiraz, Iran case study. Journal of Cleaner Production. 2019;215:1262-78.
[35] Preet S, Bhushan B, Mahajan T. Experimental investigation of water based photovoltaic/thermal (PV/T) system with and without phase change material (PCM). Sol Energy 2017;155:1104-20.
[36] Lari MO, Sahin AZ. Effect of retrofitting a silver/water nanofluid-based photovoltaic/thermal (PV/T) system with a PCM-thermal battery for residential applications. Renew Energy. 2018;122:98-107.
[37] Yang X, Sun L, Yuan Y, Zhao X, Cao X. Experimental investigation on performance comparison of PV/T-PCM system and PV/T system. Renew Energy. 2018;119:152-9.
[38] Yang X, Zhou J, Yuan Y. Energy Performance of an Encapsulated Phase Change Material PV/T System. Energies. 2019;12:3929.
[39] Ahmed R, Nabil KAI. Computational analysis of phase change material and fins effects on enhancing PV/T panel performance. J Mech Sci Technol 2017;31:3083-90.
[40] Hossain MS, Pandey AK, Selvaraj J, Rahim NA, Islam MM, Tyagi VV. Two side serpentine flow based photovoltaic-thermal-phase change materials (PVT-PCM) system: Energy, exergy and economic analysis. Renew Energy. 2019;136:1320-36.
[41] Xu H, Zhang C, Wang N, Qu Z, Zhang S. Experimental study on the performance of a solar photovoltaic/thermal system combined with phase change material. Sol Energy 2020;198:202-11.
[42] Gaur A, Ménézo C, Giroux--Julien S. Numerical studies on thermal and electrical performance of a fully wetted absorber PVT collector with PCM as a storage medium. Renew Energy. 2017;109:168-87.
[43] Al-Waeli AHA, Kazem HA, Chaichan MT, Sopian K. Experimental investigation of using nano-PCM/nanofluid on a photovoltaic thermal system (PVT): Technical and economic study. Thermal Science and Engineering Progress. 2019;11:213-30.

[44] Al-Waeli AHA, Chaichan MT, Sopian K, Kazem HA, Mahood HB, Khadom AA. Modeling and experimental validation of a PVT system using nanofluid coolant and nano-PCM. Sol Energy 2019;177:178-91.
[45] Elarga H, Goia F, Zarrella A, Dal Monte A, Benini E. Thermal and electrical performance of an integrated PV-PCM system in double skin façades: A numerical study. Sol Energy 2016;136:112-24.
[46] Fayaz H, Rahim NA, Hasanuzzaman M, Rivai A, Nasrin R. Numerical and outdoor real time experimental investigation of performance of PCM based PVT system. Sol Energy 2019;179:135-50.
[47] Fayaz H, Rahim NA, Hasanuzzaman M, Nasrin R, Rivai A. Numerical and experimental investigation of the effect of operating conditions on performance of PVT and PVT-PCM. Renew Energy. 2019;143:827-41.
[48] Al-Waeli AHA, Kazem HA, Yousif JH, Chaichan MT, Sopian K. Mathematical and neural network modeling for predicting and analyzing of nanofluid-nano PCM photovoltaic thermal systems performance. Renew Energy. 2020;145:963-80.
[49] Sardarabadi M, Passandideh-Fard M, Maghrebi M-J, Ghazikhani M. Experimental study of using both ZnO/ water nanofluid and phase change material (PCM) in photovoltaic thermal systems. Sol Energy Mater Sol Cells 2017;161:62-9.
[50] Kazemian A, Hosseinzadeh M, Sardarabadi M, Passandideh-Fard M. Experimental study of using both ethylene glycol and phase change material as coolant in photovoltaic thermal systems (PVT) from energy, exergy and entropy generation viewpoints. Energy. 2018;162:210-23.
[51] Hosseinzadeh M, Sardarabadi M, Passandideh-Fard M. Energy and exergy analysis of nanofluid based photovoltaic thermal system integrated with phase change material. Energy. 2018;147:636-47.
[52] Kazemian A, Taheri A, Sardarabadi A, Ma T, Passandideh-Fard M, Peng J. Energy, exergy and environmental analysis of glazed and unglazed PVT system integrated with phase change material: An experimental approach. Sol Energy 2020;201:178-89.
[53] Al-Waeli AHA, Sopian K, Chaichan MT, Kazem HA, Ibrahim A, Mat S, et al. Evaluation of the nanofluid and nano-PCM based photovoltaic thermal (PVT) system: An experimental study. Energy Convers Manage 2017;151:693-708.
[54] Sopian K, Al-Waeli AHA, Kazem HA. Energy, exergy and efficiency of four photovoltaic thermal collectors with different energy storage material. Journal of Energy Storage. 2020;29:101245.
[55] Maatallah T, Zachariah R, Al-Amri FG. Exergo-economic analysis of a serpentine flow type water based photovoltaic thermal system with phase change material (PVT-PCM/water). Sol Energy 2019;193:195-204.
[56] Gürel AE. Exergetic assessment of a concentrated photovoltaic thermal (CPV/T) system. Int J Exergy 2016;21:127-35.
[57] Ergün A, Eyinç H. Performance assessment of novel photovoltaic thermal system using nanoparticle in phase change material. International Journal of Numerical Methods for Heat & Fluid Flow. 2019;29:1490-505.
[58] Su Y, Zhang Y, Shu L. Experimental study of using phase change material cooling in a solar tracking concentrated photovoltaic-thermal system. Sol Energy 2018;159:777-85.
[59] Tabet Aoul K, Hassan A, Shah AH, Riaz H. Energy performance comparison of concentrated photovoltaic – Phase change material thermal (CPV-PCM/T) system with flat plate collector (FPC). Sol Energy 2018;176:453-64.
[60] Al Imam MFI, Beg RA, Rahman MS, Khan MZH. Performance of PVT solar collector with compound parabolic concentrator and phase change materials. Energy and Buildings. 2016;113:139-44.
[61] Fiorentini M, Cooper P, Ma Z. Development and optimization of an innovative HVAC system with integrated PVT and PCM thermal storage for a net-zero energy retrofitted house. Energy and Buildings. 2015;94:21-32.
[62] Xiang YT, Gan GH. Optimization of building-integrated photovoltaic thermal air system combined with thermal storage. Int J Low-Carbon Technol. 2015;10:146-56.
[63] Sudhakar P, Kumaresan G, Velraj R. Experimental analysis of solar photovoltaic unit integrated with free cool thermal energy storage system. Sol Energy 2017;158:837-44.
[64] Salem MR, Elsayed MM, Abd-Elaziz AA, Elshazly KM. Performance enhancement of the photovoltaic cells using Al2O3/PCM mixture and/or water cooling-techniques. Renew Energy. 2019;138:876-90.

[65] Karthick A, Kalidasa Murugavel K, Ghosh A, Sudhakar K, Ramanan P. Investigation of a binary eutectic mixture of phase change material for building integrated photovoltaic (BIPV) system. Sol Energy Mater Sol Cells 2020;207:110360.
[66] Karthick A, Murugavel KK, Ramanan P. Performance enhancement of a building-integrated photovoltaic module using phase change material. Energy. 2018;142:803-12.
[67] Yao J, Xu H, Dai Y, Huang M. Performance analysis of solar assisted heat pump coupled with build-in PCM heat storage based on PV/T panel. Sol Energy 2020;197:279-91.
[68] Su D, Jia Y, Alva G, Liu L, Fang G. Comparative analyses on dynamic performances of photovoltaic–thermal solar collectors integrated with phase change materials. Energy Convers Manage 2017;131:79-89.
[69] Kazemian A, Salari A, Hakkaki-Fard A, Ma T. Numerical investigation and parametric analysis of a photovoltaic thermal system integrated with phase change material. Appl Energy 2019;238:734-46.
[70] Su D, Jia YT, Lin YX, Fang GY. Maximizing the energy output of a photovoltaic-thermal solar collector incorporating phase change materials. Energy and Buildings. 2017;153:382-91.
[71] Ceylan İ, Gürel AE, Ergün A, Tabak A. Performance analysis of a concentrated photovoltaic and thermal system. Sol Energy 2016;129:217-23.
[72] Al-Musawi AIA, Taheri A, Farzanehnia A, Sardarabadi M, Passandideh-Fard M. Numerical study of the effects of nanofluids and phase-change materials in photovoltaic thermal (PVT) systems. Journal of Thermal Analysis and Calorimetry. 2019;137:623-36.
[73] Yuan W, Ji J, Modjinou M, Zhou F, Li Z, Song Z, et al. Numerical simulation and experimental validation of the solar photovoltaic/thermal system with phase change material. Appl Energy 2018;232:715-27.
[74] Browne MC, Lawlor K, Kelly A, Norton B, Cormack SJM. Indoor Characterisation of a Photovoltaic/ Thermal Phase Change Material System. Energy Procedia. 2015;70:163-71.
[75] Kazemian A, Salari A, Ma T. A year-round study of a photovoltaic thermal system integrated with phase change material in Shanghai using transient model. Energy Convers Manage 2020;210:112657.
[76] Michael JJ, Iniyan S. Performance analysis of a copper sheet laminated photovoltaic thermal collector using copper oxide – water nanofluid. Sol Energy 2015;119:439-51.
[77] Rejeb O, Sardarabadi M, Ménézo C, Passandideh-Fard M, Dhaou MH, Jemni A. Numerical and model validation of uncovered nanofluid sheet and tube type photovoltaic thermal solar system. Energy Convers Manage 2016;110:367-77.
[78] Ahmed A, Baig H, Sundaram S, Mallick TK. Use of Nanofluids in Solar PV/Thermal Systems. Int J Photoenergy 2019;2019:17.
[79] Hemmat Esfe M, Kamyab MH, Valadkhani M. Application of nanofluids and fluids in photovoltaic thermal system: An updated review. Sol Energy 2020;199:796-818.
[80] Abdelrazik AS, Al-Sulaiman FA, Saidur R, Ben-Mansour R. Evaluation of the effects of optical filtration and nanoPCM on the performance of a hybrid photovoltaic-thermal solar collector. Energy Convers Manage 2019;195:139-56.
[81] Manigandan S, Kumar V. Comparative study to use nanofluid ZnO and CuO with phase change material in photovoltaic thermal system. Int J Energy Res 2019;43:1882-91.
[82] Salari A, Kazemian A, Ma T, Hakkaki-Fard A, Peng J. Nanofluid based photovoltaic thermal systems integrated with phase change materials: Numerical simulation and thermodynamic analysis. Energy Convers Manage 2020;205:112384.
[83] Al-Waeli AHA, Sopian K, Kazem HA, Yousif JH, Chaichan MT, Ibrahim A, et al. Comparison of prediction methods of PV/T nanofluid and nano-PCM system using a measured dataset and artificial neural network. Sol Energy 2018;162:378-96.
[84] Sarafraz MM, Safaei MR, Leon AS, Tlili I, Alkanhal TA, Tian Z, et al. Experimental Investigation on Thermal Performance of a PV/T-PCM (Photovoltaic/Thermal) System Cooling with a PCM and Nanofluid. Energies. 2019;12:16.
[85] Waqas A, Ji J, Xu L, Ali M, Zeashan, Alvi J. Thermal and electrical management of photovoltaic panels using phase change materials – A review. Renew Sust Energ Rev. 2018;92:254-71.
[86] Huang MJ, Eames PC, Norton B, Hewitt NJ. Natural convection in an internally finned phase change material heat sink for the thermal management of photovoltaics. Sol Energy Mater Sol Cells 2011;95:1598-603.

[87] Simón-Allué R, Guedea I, Villén R, Brun G. Experimental study of Phase Change Material influence on different models of Photovoltaic-Thermal collectors. Sol Energy 2019;190:1-9.
[88] Salunkhe PB, Shembekar PS. A review on effect of phase change material encapsulation on the thermal performance of a system. Renew Sust Energ Rev. 2012;16:5603-16.
[89] Yao Y, Wu H. Pore-scale simulation of melting process of paraffin with volume change in high porosity open-cell metal foam. Int J Therm Sci 2019;138:322-40.
[90] Huang X, Lin Y, Alva G, Fang G. Thermal properties and thermal conductivity enhancement of composite phase change materials using myristyl alcohol/metal foam for solar thermal storage. Sol Energy Mater Sol Cells 2017;170:68-76.
[91] Yang X, Yu J, Guo Z, Jin L, He Y-L. Role of porous metal foam on the heat transfer enhancement for a thermal energy storage tube. Appl Energy 2019;239:142-56.
[92] Wang G, Wei G, Xu C, Ju X, Yang Y, Du X. Numerical simulation of effective thermal conductivity and pore-scale melting process of PCMs in foam metals. Appl Therm Eng 2019;147:464-72.
[93] Tauseef ur R, Ali HM, Janjua MM, Sajjad U, Yan W-M. A critical review on heat transfer augmentation of phase change materials embedded with porous materials/foams. Int J Heat Mass Transf. 2019;135:649-73.
[94] Yang X, Guo Z, Liu Y, Jin L, He Y-L. Effect of inclination on the thermal response of composite phase change materials for thermal energy storage. Appl Energy 2019;238:22-33.
[95] Peng H, Zhang D, Ling X, Li Y, Wang Y, Yu Q, et al. n-Alkanes Phase Change Materials and Their Microencapsulation for Thermal Energy Storage: A Critical Review. Energy & Fuels. 2018;32:7262-93.
[96] Zhang Y, Baiocco D, Mustapha AN, Zhang X, Yu Q, Wellio G, et al. Hydrocolloids: Nova materials assisting encapsulation of volatile phase change materials for cryogenic energy transport and storage. Chemical Engineering Journal. 2020;382:123028.
[97] Yu Q, Romagnoli A, Al-Duri B, Xie D, Ding Y, Li Y. Heat storage performance analysis and parameter design for encapsulated phase change materials. Energy Convers Manage 2018;157:619-30.
[98] Yu Q, Tchuenbou-Magaia F, Al-Duri B, Zhang Z, Ding Y, Li Y. Thermo-mechanical analysis of microcapsules containing phase change materials for cold storage. Appl Energy 2018;211:1190-202.
[99] Delgado M, Lázaro A, Mazo J, Zalba B. Review on phase change material emulsions and microencapsulated phase change material slurries: Materials, heat transfer studies and applications. Renew Sust Energ Rev. 2012;16:253-73.
[100] Zhang Y, Wang S, Rao Z, Xie J. Experiment on heat storage characteristic of microencapsulated phase change material slurry. Sol Energy Mater Sol Cells 2011;95:2726-33.
[101] Delgado M, Lázaro A, Mazo J, Marín JM, Zalba B. Experimental analysis of a microencapsulated PCM slurry as thermal storage system and as heat transfer fluid in laminar flow. Appl Therm Eng 2012;36:370-7.
[102] Huang X, Zhu C, Lin Y, Fang G. Thermal properties and applications of microencapsulated PCM for thermal energy storage: A review. Appl Therm Eng 2019;147:841-55.
[103] Liu L, Jia Y, Lin Y, Alva G, Fang G. Performance evaluation of a novel solar photovoltaic–thermal collector with dual channel using microencapsulated phase change slurry as cooling fluid. Energy Convers Manage 2017;145:30-40.
[104] Jia YT, Zhu CQ, Fang GY. Performance optimization of a photovoltaic/thermal collector using microencapsulated phase change slurry. Int J Energy Res 2020;44:1812-27.
[105] Liu L, Jia Y, Lin Y, Alva G, Fang G. Numerical study of a novel miniature compound parabolic concentrating photovoltaic/thermal collector with microencapsulated phase change slurry. Energy Convers Manage 2017;153:106-14.
[106] Yu Q, Romagnoli A, Yang R, Xie D, Liu C, Ding Y, et al. Numerical study on energy and exergy performances of a microencapsulated phase change material slurry based photovoltaic/thermal module. Energy Convers Manage 2019;183:708-20.
[107] Eisapour M, Eisapour AH, Hosseini MJ, Talebizadehsardari P. Exergy and energy analysis of wavy tubes photovoltaic-thermal systems using microencapsulated PCM nano-slurry coolant fluid. Appl Energy 2020;266:114849.

[108] Chen HB, Gong YT, Wei P, Nie PJ, Xiong YX, Wang CC. Experimental Study on the Performance of a Phase Change Slurry-Based Heat Pipe Solar Photovoltaic/Thermal Cogeneration System. Int J Photoenergy 2019:10.
[109] Qiu Z, Ma X, Zhao X, Li P, Ali S. Experimental investigation of the energy performance of a novel Micro-encapsulated Phase Change Material (MPCM) slurry based PV/T system. Appl Energy 2016;165:260-71.
[110] Roaf S, Brotas L, Nicol F. Counting the costs of comfort. Building Research & Information. 2015;43:269-73.
[111] Yang T, Athienitis AK. A review of research and developments of building-integrated photovoltaic/thermal (BIPV/T) systems. Renew Sust Energ Rev. 2016;66:886-912.
[112] Yin HM, Yang DJ, Kelly G, Garant J. Design and performance of a novel building integrated PV/thermal system for energy efficiency of buildings. Sol Energy 2013;87:184-95.
[113] Fiorentini M, Cooper P, Ma Z, Robinson DA. Hybrid Model Predictive Control of a Residential HVAC System with PVT Energy Generation and PCM Thermal Storage. Energy Procedia. 2015;83:21-30.
[114] Ren HS, Lin WY, Ma ZJ, Fan WK. Thermal performance evaluation of an integrated photovoltaic thermal-phase change material system using Taguchi method. Energy Procedia. 2017;121:118-25.
[115] Lin W, Ma Z, Sohel MI, Cooper P. Development and evaluation of a ceiling ventilation system enhanced by solar photovoltaic thermal collectors and phase change materials. Energy Convers Manage 2014;88:218-30.
[116] Lin WY, Ma ZJ, Cooper P, Sohel MI, Yang LW. Thermal performance investigation and optimization of buildings with integrated phase change materials and solar photovoltaic thermal collectors. Energy and Buildings. 2016;116:562-73.
[117] Lin WY, Ma ZJ. Using Taguchi-Fibonacci search method to optimize phase change materials enhanced buildings with integrated solar photovoltaic thermal collectors. Energy. 2016;106:23-37.
[118] Zhou Y, Liu X, Zhang G. Performance of buildings integrated with a photovoltaic–thermal collector and phase change materials. Procedia Engineering. 2017;205:1337-43.
[119] Liu XH, Zhou YK, Li CQ, Lin YL, Yang W, Zhang GQ. Optimization of a New Phase Change Material Integrated Photovoltaic/Thermal Panel with The Active Cooling Technique Using Taguchi Method. Energies. 2019;12:22.
[120] Aelenei L, Pereira R, Gonçalves H, Athienitis A. Thermal Performance of a Hybrid BIPV-PCM: Modeling, Design and Experimental Investigation. Energy Procedia. 2014;48:474-83.
[121] Pereira R, Aelenei L. Optimization assessment of the energy performance of a BIPV/T-PCM system using Genetic Algorithms. Renew Energy. 2019;137:157-66.
[122] Čurpek J, Čekon M. Climate response of a BiPV façade system enhanced with latent PCM-based thermal energy storage. Renew Energy. 2020;152:368-84.
[123] Long H, Chow T-T, Ji J. Building-integrated heat pipe photovoltaic/thermal system for use in Hong Kong. Sol Energy 2017;155:1084-91.
[124] Hu M, Zheng R, Pei G, Wang Y, Li J, Ji J. Experimental study of the effect of inclination angle on the thermal performance of heat pipe photovoltaic/thermal (PV/T) systems with wickless heat pipe and wire-meshed heat pipe. Appl Therm Eng 2016;106:651-60.
[125] Zhang T, Yan ZW, Xiao L, Fu HD, Pei G, Ji J. Experimental, study and design sensitivity analysis of a heat pipe photovoltaic/thermal system. Appl Therm Eng 2019;162:114318.
[126] Chen H, Zhang H, Li M, Liu H, Huang J. Experimental investigation of a novel LCPV/T system with micro-channel heat pipe array. Renew Energy. 2018;115:773-82.
[127] Ren X, Yu M, Zhao X, Li J, Zheng S, Chen F, et al. Assessment of the cost reduction potential of a novel loop-heat-pipe solar photovoltaic/thermal system by employing the distributed parameter model. Energy. 2020;190:116338.
[128] Sweidan A, Ghaddar N, Ghali K. Optimized design and operation of heat-pipe photovoltaic thermal system with phase change material for thermal storage. Journal of Renewable and Sustainable Energy. 2016;8:023501.
[129] Diallo TMO, Yu M, Zhou J, Zhao X, Shittu S, Li G, et al. Energy performance analysis of a novel solar PVT loop heat pipe employing a microchannel heat pipe evaporator and a PCM triple heat exchanger. Energy. 2019;167:866-88.

[130] Wang Z, Huang Z, Chen F, Zhao X, Guo P. The integration of solid-solid phase change material with micro-channel flat plate heat pipe-based BIPV/T. Build Serv Eng Res Technol. 2018;39:712-32.
[131] Wang Z, Huang Z, Chen F, Zhao X, Guo P. Experimental investigation of the novel BIPV/T system employing micro-channel flat-plate heat pipes. Build Serv Eng Res Technol. 2018;39:540-56.
[132] Kılkış B. Development of a composite PVT panel with PCM embodiment, TEG modules, flat-plate solar collector, and thermally pulsing heat pipes. Sol Energy 2020;200:89-107.
[133] Zhang J, Zhai H, Wu Z, Wang Y, Xie H. Experimental investigation of novel integrated photovoltaic-thermoelectric hybrid devices with enhanced performance. Sol Energy Mater Sol Cells 2020;215:110666.
[134] Zhao Q, Zhang H, Hu Z, Hou S. Achieving a broad-spectrum photovoltaic system by hybridizing a two-stage thermoelectric generator. Energy Convers Manage 2020;211:112778.
[135] Cui YJ, Wang BL, Li JE, Wang KF. Performance evaluation and lifetime prediction of a segmented photovoltaic-thermoelectric hybrid system. Energy Convers Manage 2020;211:112744.
[136] Li G, Shittu S, zhou K, Zhao X, Ma X. Preliminary experiment on a novel photovoltaic-thermoelectric system in summer. Energy. 2019;188:116041.
[137] Zhang J, Zhai H, Wu Z, Wang Y, Xie H, Zhang M. Enhanced performance of photovoltaic–thermoelectric coupling devices with thermal interface materials. Energy Reports. 2020;6:116-22.
[138] Cui T, Xuan Y, Yin E, Li Q, Li D. Experimental investigation on potential of a concentrated photovoltaic-thermoelectric system with phase change materials. Energy. 2017;122:94-102.
[139] Motiei P, Yaghoubi M, GoshtasbiRad E. Transient simulation of a hybrid photovoltaic-thermoelectric system using a phase change material. Sustainable Energy Technologies and Assessments. 2019;34:200-13.
[140] Vaishak S, Bhale PV. Photovoltaic/thermal-solar assisted heat pump system: Current status and future prospects. Sol Energy 2019;189:268-84.
[141] Xiang B, Ji Y, Yuan Y, Wu D, Zeng C, Zhou J. 10-year simulation of photovoltaic-thermal road assisted ground source heat pump system for accommodation building heating in expressway service area. Sol Energy 2021;215:459-72.
[142] Yao J, Zheng S, Chen D, Dai Y, Huang M. Performance improvement of vapor-injection heat pump system by employing PVT collector/evaporator for residential heating in cold climate region. Energy. 2021;219:119636.
[143] Öztürk M, Çalişir O, Genç G. Energy, exergy and economic (3E) evaluation of the photovoltaic/thermal collector-assisted heat pump domestic water heating system for different climatic regions in Turkey. Journal of Thermal Analysis and Calorimetry. 2021.
[144] James A, Mohanraj M, Srinivas M, Jayaraj S. Thermal analysis of heat pump systems using photovoltaic-thermal collectors: a review. Journal of Thermal Analysis and Calorimetry. 2021;144:1-39.
[145] Bigaila E, Athienitis AK. Modeling and simulation of a photovoltaic/thermal air collector assisting a façade integrated small scale heat pump with radiant PCM panel. Energy and Buildings. 2017;149:298-309.
[146] Tashtoush BM, Al-Nimr MdA, Khasawneh MA. A comprehensive review of ejector design, performance, and applications. Appl Energy 2019;240:138-72.
[147] Braimakis K. Solar ejector cooling systems: A review. Renew Energy. 2021;164:566-602.
[148] Ghorbani B, Mehrpooya M, Sharifzadeh MMM. Introducing a hybrid photovoltaic-thermal collector, ejector refrigeration cycle and phase change material storage energy system (Energy, exergy and economic analysis). International Journal of Refrigeration-Revue Internationale Du Froid. 2019;103:61-76.
[149] Ma T, Li M, Kazemian A. Photovoltaic thermal module and solar thermal collector connected in series to produce electricity and high-grade heat simultaneously. Appl Energy 2020;261:114380.
[150] Al-harahsheh M, Abu-Arabi M, Mousa H, Alzghoul Z. Solar desalination using solar still enhanced by external solar collector and PCM. Appl Therm Eng 2018;128:1030-40.
[151] Yousef MS, Hassan H. Energetic and exergetic performance assessment of the inclusion of phase change materials (PCM) in a solar distillation system. Energy Convers Manage 2019;179:349-61.
[152] Xiao L, Shi R, Wu S-Y, Chen Z-L. Performance study on a photovoltaic thermal (PV/T) stepped solar still with a bottom channel. Desalination. 2019;471:114129.

[153] Hedayati-Mehdiabadi E, Sarhaddi F, Sobhnamayan F. Exergy performance evaluation of a basin-type double-slope solar still equipped with phase-change material and PV/T collector. Renew Energy. 2020;145:2409-25.
[154] Rosen MA, Koohi-Fayegh S. The prospects for hydrogen as an energy carrier: an overview of hydrogen energy and hydrogen energy systems. Energy, Ecology and Environment. 2016;1:10-29.
[155] Oruc ME, Desai AV, Kenis PJA, Nuzzo RG. Comprehensive energy analysis of a photovoltaic thermal water electrolyzer. Appl Energy 2016;164:294-302.
[156] Cilogluları M, Erden M, Karakilcik M, Dincer I. Investigation of hydrogen production performance of a Photovoltaic and Thermal System. International Journal of Hydrogen Energy. 2017;42:2547-52.
[157] Shafiei Kaleibari S, Yanping Z, Abanades S. Solar-driven high temperature hydrogen production via integrated spectrally split concentrated photovoltaics (SSCPV) and solar power tower. International Journal of Hydrogen Energy. 2019;44:2519-32.